Published online 6 January 2016 *Nucleic Acids Research, 2016, Vol. 44, No. 9* ***4105–4122***
doi: 10.1093/nar/gkv1528

Integrative analysis identifies targetable CREB1/FoxA1 transcriptional co-regulation as a predictor of prostate cancer recurrence

Benjamin Sunkel[1,2,3,†], Dayong Wu[2,3,†], Zhong Chen[2,3], Chiou-Miin Wang[4], Xiangtao Liu[3], Zhenqing Ye[4], Aaron M. Horning[4], Joseph Liu[4], Devalingam Mahalingam[4], Horacio Lopez-Nicora[5], Chun-Lin Lin[4], Paul J. Goodfellow[3], Steven K. Clinton[3,6], Victor X. Jin[4], Chun-Liang Chen[4], Tim H.-M. Huang[4] and Qianben Wang[1,2,3,*]

[1]Ohio State Biochemistry Program, The Ohio State University, Columbus, OH 43210, USA, [2]Department of Molecular Virology, Immunology and Medical Genetics, The Ohio State University, Columbus, OH 43210, USA, [3]The Ohio State University Comprehensive Cancer Center, Columbus, OH 43210, USA, [4]Department of Molecular Medicine, University of Texas Health Science Center at San Antonio, San Antonio, TX 78229, USA, [5]Department of Plant Pathology, The Ohio State University, Columbus, OH 43210, USA and [6]Division of Medical Oncology, Department of Internal Medicine, The Ohio State University, Columbus, OH 43210, USA

Received September 30, 2015; Revised December 6, 2015; Accepted December 22, 2015

ABSTRACT

Identifying prostate cancer-driving transcription factors (TFs) in addition to the androgen receptor promises to improve our ability to effectively diagnose and treat this disease. We employed an integrative genomics analysis of master TFs CREB1 and FoxA1 in androgen-dependent prostate cancer (ADPC) and castration-resistant prostate cancer (CRPC) cell lines, primary prostate cancer tissues and circulating tumor cells (CTCs) to investigate their role in defining prostate cancer gene expression profiles. Combining genome-wide binding site and gene expression profiles we define CREB1 as a critical driver of pro-survival, cell cycle and metabolic transcription programs. We show that CREB1 and FoxA1 co-localize and mutually influence each other's binding to define disease-driving transcription profiles associated with advanced prostate cancer. Gene expression analysis in human prostate cancer samples found that CREB1/FoxA1 target gene panels predict prostate cancer recurrence. Finally, we showed that this signaling pathway is sensitive to compounds that inhibit the transcription co-regulatory factor MED1. These findings not only reveal a novel, global transcriptional co-regulatory function of CREB1 and FoxA1, but also suggest CREB1/FoxA1 signaling is a targetable driver of prostate cancer progression and serves as a biomarker of poor clinical outcomes.

INTRODUCTION

The complexity, heterogeneity and plasticity of prostate cancer have proven major obstacles in our understanding of the etiology and progression of this disease (1,2), and have provided a rich source for discovery of novel cancer concepts and a platform for the development of new analytical methods (3). Critical questions remain as to the optimal approaches to characterize aggressive versus indolent disease in the clinically localized setting, the factors that predict treatment response and failure, and the mechanisms underlying therapeutic failure that reveal novel targets for effective intervention. Specifically, the discovery of targetable prostate cancer drivers outside the androgen/androgen receptor (AR) signaling axis is paramount to achieving cures and improving the duration of therapeutic response. The importance of this concept is made increasingly apparent by the mounting reports of resistance to even the most potent second-generation antiandrogen therapeutics and continually emerging molecular mechanisms underlying such treatment failure (4).

Genomic analyses of primary and advanced metastatic prostate cancers have endeavored to reveal the alterations characterizing aggressive disease in hopes of identifying novel driver genes and pathways (1,2,5,6). While potentially clinically actionable mutations in PI3K (*PIK3CB*), RAF, DNA repair (*ATM* and *BRCA1/2*) and cell cycle (*CDK4*)

*To whom correspondence should be addressed. Qianben Wang. Tel: +1 614 247 1609; Fax: +1 614 688 4181; Email: qianben.wang@osumc.edu
†These authors contributed equally to the paper as first authors.

pathways were discovered in metastatic CRPC patient samples (7), primary cancer studies have returned few therapeutic candidates beyond AR itself. Additionally, while genome-wide copy number alteration (CNA) alone or in combination with additional tumor characteristics provide valuable prognostic information for effective risk stratification to aid in early clinical decision making (8,9), they do not immediately identify the therapeutic compounds from which a high-risk prostate cancer patient may benefit. These observations encourage an alternate, mechanistic approach to the discovery of targetable disease-driving pathways that can simultaneously predict risk and indicate potential therapeutic strategies early in the course of treatment.

Our recent analysis of the pioneer transcription factor FoxA1 revealed its collaborative relationship with the cAMP response element binding protein (CREB1) in determining the expression of G1/S phase cell cycle progression genes (10). Additionally, these factors support the androgen-independent AR-mediated expression of G2/M phase cell cycle enhancers in CRPC cells. These results suggest that comprehensive analysis of genome-wide CREB1/FoxA1 cooperativity may define disease-relevant gene expression profiles during the evolution and progression of human prostate cancer.

Individually, while FoxA1 has been well characterized, CREB1-mediated transcription remains largely unexplored in prostate cancer. This important second messenger-responsive transcription factor (TF), in addition to promoting cell cycle progression, has been implicated in several prostate cancer-relevant functions including steroidogenesis (11) and bone metastasis (12). CREB1 is also emerging as a key mediator of metabolic programs in cancer cells, orchestrating the response to metabolic stress and multiple extracellular hormonal signals (13). Its kinase-inducible transactivation, minimally by Serine 133 phosphorylation resulting in CREB binding protein (CBP)/p300 recruitment to target gene loci, can be stimulated by multiple signaling pathways, some of which are deregulated in prostate cancer (ex. IGF-I and PI3K/Akt) (14). Consequently, CREB1 signaling represents an attractive therapeutic candidate. Complete profiling of CREB1 target genes should therefore expand on these insights and provide a rationale for the development and use of direct or indirect CREB1-inhibiting compounds in prostate cancer prevention or therapy.

Utilizing the LNCaP and abl cell lines, which model hormone-dependent and -independent growth characteristics as well as the clinical properties of a significant portion of ADPC (androgen-dependent prostate cancer) and CRPC (castration-resistant prostate cancer) patients, respectively (10,15–17), the current study is the first to explore genome-wide CREB1 signaling individually and in collaboration with FoxA1. Our integrated genomics approach compiles CREB1 and FoxA1 binding site data with gene expression profiles of transcripts responsive to individual TF silencing to characterize cooperative CREB1/FoxA1 transcriptional activity. We also utilize these genomic datasets in a knowledge-driven approach to the discovery of prognostic gene panels. We have demonstrated that coordinated CREB1/FoxA1 signaling contributes to disease-relevant transcription programs in both ADPC and CRPC cells. We further show that CRPC-associated CREB1/FoxA1 target genes provide valuable tools for assessing risk of prostate cancer recurrence in primary patient tissues. Importantly, we demonstrate that CREB1/FoxA1 transcriptional activity is sensitive to kinase inhibitors that impact the transcription co-regulator MED1. We propose that this work reveals a potentially targetable transcription regulatory signaling axis that may serve as a robust biomarker of disease recurrence.

MATERIALS AND METHODS

Cell culture

LNCaP and 22rv1 cells were purchased from American Type Culture Collection (ATCC), and maintained in RPMI 1640 or DMEM, respectively, supplemented with 10% FBS. The abl cell line was kindly provided by Zoran Culig (Innsbruck Medical University, Austria; (18)), and maintained in phenol red-free RPMI 1640 supplemented with 10% charcoal-stripped FBS. Individual experiments were conducted in phenol red-free RPMI 1640 or DMEM supplemented with 5% charcoal-stripped FBS.

Quantitative RT-PCR

Real-time reverse transcriptase (qRT)-PCR was carried out as previously described (19). Cells were treated with vehicle, 5 or 10 μM H89, 10 μM U0126, or 3 μM MK-2206 for 24 h prior to collection or with Control- (Dharmacon ON-TARGETplus Non-targeting Pool, D-001810–10–20) or AR- (Dharmacon ON-TARGETplus, L-003400–00–0020) targeting siRNA for 72 h prior to collection. Total RNA was isolated with the RNeasy Mini kit (Qiagen, 74104). qRT-PCR was conducted using the MultiScribe Reverse Transcriptase and Power SYBR Green PCR Master Mix reagents (Applied Biosystems), according to the manufacturer's instructions. Each assay was repeated three to four times. The qRT-PCR primers for *in vitro* assays are listed in (Supplementary Table S1A).

Western blotting

Western blot analyses were carried out as previously described (19). Briefly, cells were collected and lysed in RIPA buffer (1% NP-40, 0.1% sodium dodecyl sulphate (SDS), 50 mM Tris–HCl pH 7.4, 150 mM NaCl, 0.5% Sodium Deoxycholate, 1 mM ethylenediaminetetraacetic acid (EDTA), 1× proteinase inhibitor cocktail (Roche), 1× PhosSTOP phosphatase inhibitor cocktail (Roche)) for 20 min on ice and the proteins were resolved on 8% SDS-polyacrylamide gels before being transferred onto Nitrocellulose membrane (Bio-Rad). The membrane was blocked with 5% milk powder (Bio-Rad) then incubated with specific antibodies against Ser133 phospho-CREB (87G3), CREB1 (48H2), Thr202/Tyr204 phospho-Erk1/2 (9101), Erk1/2 (9102), Ser472 phospho-Akt (D9E) and Akt (C67E7) (Cell Signaling Technology), AR (N-20), GAPDH (6C5) and TRAP220/MED1 (C-19) (Santa Cruz), FoxA1 (ab23738) (Abcam), Calnexin (ADI-SPA-860) (Enzo) or our own Thr1032 phospho-MED1 antibody (YenZyme) (15) for 2 h at room temperature. Following incubation with secondary antibodies, immunoblots were visualized using the C-DiGit Chemiluminescent Western Blot Scanner (Li-Cor).

ChIP-qPCR

ChIP-qPCR was performed as previously described (19). For kinase inhibitor assays, cells were treated with vehicle, 10 μM H89 or 10 μM U0126 24 h prior to collection. For siCREB1 FoxA1 ChIP, cells were transfected with Control- (Dharmacon ON-TARGETplus Non-targeting Pool, D-001810–10–20) or CREB1- (Dharmacon, SMARTPool: ON-TARGETplus, L-003619–00–0005) targeting siRNA 72 h before collection using Lipofectamine 2000. For CREB1 overexpression ChIP, cells were transfected with Control (pCMV-LacZ—Clontech) or wild-type CREB1 (pCMV-CREB—Clontech) expression vectors 48 h prior to collection with Lipofectamine 2000. Cells were then crosslinked with 1% formaldehyde for 10 min at room temperature and chromatin was collected, sonicated, diluted and immunoprecipitated with 4 μg of specific antibodies against CREB1 (ab31387) and H3K27ac (ab4729) (Abcam), CBP (C-20), p300 (C-20) and RNA polymerase II (Pol II) (N-20) (Santa Cruz), and pMED1 (YenZyme) (15) at 4°C overnight. Protein A-Sepharose beads were added and incubated for 1 h with rotation. The beads were washed sequentially for 10 min each in TSE I (0.1% SDS, 1% Triton X-100, 2 mM EDTA, 20 mM Tris–HCl, pH 8.1, 150 mM NaCl), TSE II (0.1% SDS, 1% Triton X-100, 2 mM EDTA, 20 mM Tris–HCl, pH 8.1, 500 mM NaCl), and buffer III (0.25 M LiCl, 1% NP-40, 1% deoxycholate, 1 mM EDTA, 10 mM Tris–HCl, pH 8.1) and finally two times with TE buffer. Chromatin complexes were eluted in 1% SDS, 0.1 M NaHCO3 and decrosslinked at 65°C for 16 h. DNA fragments were purified with the QIAquick PCR purification kit (Qiagen 28104) and used as the template in quantitative PCR reactions with Power SYBR Green PCR Master Mix reagents (Applied Biosystems). ChIP-qPCR primers are listed in (Supplementary Table S1A). ChIP assays were replicated two to three times.

ChIP-seq

ChIP-seq was performed as previously described (19). Briefly, 10^7 cells were cross-linked in 1% formaldehyde for 10 min at room temperature. Chromatin was sheared, diluted, incubated with specific antibodies against CREB1 (ab31387) or FoxA1 (ab23738) (Abcam), and precipitated with Protein A-Sepharose beads. ChIP-seq library preparation was performed using the Illumina Truseq ChIP Sample Preparation Kit (part# 15023092) with up to 10 ng of purified ChIP-enriched DNA. The libraries were amplified using 15 PCR cycles, and 50 bp single-end reads were generated on the Illumina HiSeq 2500 platform at the Ohio State University Comprehensive Cancer Center (OSUCCC) sequencing core with four multiplexed samples per lane. ChIP-seq reads were aligned to the human reference genome (hg19) with Bowtie v1.0.0, allowing at most two mismatches. Uniquely mapped reads were utilized for peak calling using MACS v1.4.2 with *P*-value threshold of 10^{-8}. Aligned reads heatmaps and average signal plots were generated on the Galaxy platform using the Heatmap and SitePro functions. Motif analysis was performed using SeqPos on the Galaxy platform as well as Homer. Motif scanning was performed using Bio.motifs. For siCREB1 and siFoxA1 ChIP-seq, abl cells were transfected with Control- (Dharmacon ON-TARGETplus Non-targeting Pool, D-001810–10–20), CREB1- (Dharmacon, SMARTPool: ON-TARGETplus, L-003619–00–0005), or FoxA1- (Dharmacon, SMARTPool: ON-TARGETplus, L-010319–00–0005) targeting siRNA using Lipofectamine 2000 per the manufacturer's protocol. Seventy-two hours following transfection, CREB1 ChIP-seq was performed as described above in siControl and siFoxA1 transfected cells while FoxA1 ChIP-seq was performed in siControl and siCREB1 transfected cells. All ChIP-seq experiments were conducted in duplicate.

RNA-seq

LNCaP and abl cells were transfected with Control-, CREB1- or FoxA1-targeting siRNAs using Lipofectamine 2000 per the manufacturer's protocol. Seventy-two hours following transfection, RNA was harvested using the RNeasy Mini Kit (Qiagen). cDNA libraries were prepared using the Illumina Truseq RNA Sample Prep Kit (part# RS-122–2001) according to the manufacturer's protocol. A total of 50 bp single-end reads were generated on the Illumina HiSeq 2500 platform at the OSUCCC sequencing core with three multiplexed samples per lane. Read alignment was conducted using TopHat 2.0.8 (Bowtie2 2.1.0) and relative transcript abundances were calculated using HTSeq 0.5.3p9. edgeR 3.0.6 was used to identify differentially expressed genes between LNCaP and abl cells (siControl versus siControl) and after TF silencing in both LNCaP and abl cells (siCREB1 versus siControl and siFoxA1 versus siControl). All RNA-seq assays were conducted in duplicate.

Target gene identification

The Genomic Regions Enrichment of Annotations Tool (GREAT) was used to collect all genes ±50 kb from all CREB1 or FoxA1 binding sites in LNCaP and abl cells. Resulting gene lists were filtered based on responsiveness to siCREB1 or siFoxA1 transfection compared to siControl ([Fold Change] $\geq$1.2, *P*-value $\leq$ 0.05, FDR $\leq$ 5%). Complementary gene identification approach began by classifying three sets of genes by their response to siCREB1 and siFoxA1 transfection (upregulated, downregulated and unchanged by silencing of both TFs); ±20 kb from the transcription start site of all such genes, we identified solo CREB1 or FoxA1 binding sites, non-overlapping CREB1 + FoxA1 binding sites and overlapping CREB1/FoxA1 binding sites. Responsive genes with either overlapping or non-overlapping binding were defined as co-regulated genes.

Gene expression analysis in circulating tumor cells

Patient consent and blood collection were processed according to IRB protocol approved at the University of Texas Health Science Center at San Antonio. Fifteen castration-resistant (CR) and 10 castration sensitive (CS) patients were included in our cohort, with ∼12 circulating tumor cells (CTCs) measured per patient (Supplementary Table S1B). CTCs were isolated by microfiltration and immunostaining for EpCAM and CD45 following the method

described previously with minor modifications (20). CTCs were retrieved from *ScreenCell* filters with a micromanipulator and stored in 4.7 μl 2× reaction buffer at −80°C until further processing. Expression profiling of the 25 Panel A and B genes and a control gene, *UBB*, in CTCs was carried out in duplicate using microfluidic qRT-PCR as described previously (21). Primer sequences were obtained from PrimerBank and synthesized by Sigma (Supplementary Table S1C). Frozen, single CTCs were thawed on ice and the volume was diluted with 5 μl H_2O. A total of 3 μl of lysate were used for preamplification and microfluidic qRT-PCR. Average gene expression levels were calculated using the -$\Delta\Delta C_t$ method. A Mann–Whitney U test was applied to analyze differences in expression levels between CR and CS patients for each gene (Supplementary Table S1D).

Data analysis

Statistical tests, clustering analysis, Cox regression and logistic regression were performed using JMP version 10.0.2 and R version 3.1.1 with publicly available expression array data downloaded from the Gene Expression Omnibus (GEO) (Taylor—GSE21036) or provided by Glinsky *et al.* (22). Gene ontology was performed using DAVID. To assemble our gene panels, we first prioritized up- and downregulated genes that were common to multiple ONCOMINE concepts to extract four relatively small gene lists representing CREB1/FoxA1 up- and downregulated genes from LNCaP and abl cells. Utilizing cBioPortal (23), we further refined these lists to include only those genes exhibiting highly coordinated expression within each panel using data from Taylor *et al.* (6). Gene panel expression was calculated as the sum of gene ranks (with respect to all genes measured in a given data set) for all genes within a panel. For genes with multiple probes, average gene ranks were utilized. Panel A and Panel B rank sums were then converted to a Z-score for each patient.

RESULTS

CREB1 transcriptional activity in prostate cancer models

Being uncharacterized with respect to its genome-wide transcriptional activity during the evolution of prostate cancer, we began the current study with a comprehensive identification of CREB1 target genes in LNCaP and abl cells. CREB1 ChIP-seq assays identified a large set of common ($n = 18\,433$) and cell type-specific (abl: $n = 9196$, LNCaP: $n = 3391$) binding sites occupied by CREB1 in the absence of androgen at a significance threshold level of 10^{-8} (Figure 1A and B). We had previously reported that total CREB1 expression is elevated in abl compared to LNCaP cells (10). Noting that the majority of cell type-specific CREB1 binding sites were found in abl, we asked if elevated CREB1 expression might explain this observation. Overexpression of wild-type CREB1 in LNCaP cells induced a marginal increase in CREB1 binding at abl-specific sites, though LNCaP CREB1 occupancy never achieved the level observed in abl at these same regions (Supplementary Figure S1A and B). On the other hand, at common CREB1 binding sites in the *CCNE2* and *E2F1* promoter regions, which exhibit elevated CREB1 occupancy in abl, CREB1 overexpression in LNCaP resulted in stronger CREB1 binding that matched the levels observed in abl cells (Supplementary Figure S1B). These results suggest that CREB1 expression level is just one factor determining the distribution and intensity of CREB1 binding sites.

We found that common CREB1 binding sites were primarily located in proximal, gene promoter regions (51.6%), while cell line-specific binding sites most often mapped further than 5 kb from the nearest transcription start site (TSS) (cumulatively 83.5 and 85.1% for LNCaP-specific and abl-specific, respectively) (Figure 1C). While the overall proportion of CREB1 distal binding events in LNCaP cells (∼13.2%) is consistent with previous genome-wide analyses for this TF in other systems (24), the proportion of distal binding sites increases more than two-fold in abl cells (∼28.6%), providing an example of high frequency, distal CREB1 binding not previously reported. Analyzing additional ChIP-seq datasets (17,25) (Z.C. and Q.W.), we observed that common CREB1 binding sites indeed resembled active promoters marked by concurrent histone H3 lysine 4 di- and trimethylation (H3K4me2 and H3K4me3, respectively), with robust RNA Polymerase II (Pol II) enrichment (Figure 1D). These regions were depleted of repressive H3 lysine 27 trimethylation (H3K27me3), which shows robust accumulation over the TSS of silent compared to highly expressed genes in LNCaP and abl cells (Supplementary Figure S1C). On the other hand, cell line-specific CREB1 binding sites displayed an active enhancer signature characterized by H3K4me2 and Pol II enrichment in the absence of both H3K4me3 and H3K27me3 (Figure 1D) (26).

This intriguing result lead us to ask whether cell line-specific enhancer binding of CREB1 corresponds with differential gene expression profiles in LNCaP versus abl cells. We therefore conducted RNA-seq following transfection with CREB1- or control-targeting siRNA and identified the genes nearest common and cell type-specific CREB1 binding sites that were responsive to CREB1 silencing (i.e. putative target genes) using the genomic regions enrichment of annotations tool (GREAT) (Supplementary Table S2A) (27). Using the siControl RNA-seq data in LNCaP and abl cells, we then analyzed the basal expression level of these CREB1 target genes to find that cell line-specific enhancer binding of CREB1 corresponds to a higher degree of differential gene expression (proportion of differentially expressed genes: LNCaP-specific = 0.327, abl-specific 0.245) compared to common CREB1 binding in promoter regions (proportion of differentially expressed genes = 0.118) (Exact binomial test P-value $< 10^{-16}$) (Supplementary Figure S2A). Gene ontology analysis revealed that differentially expressed genes upregulated by abl-specific CREB1 binding sites were enriched for cell cycle processes, and genes down-regulated in either cell line by LNCaP- or abl-specific CREB1 binding were in enriched in apoptotic signaling. On the other hand, genes occupied by common CREB1 binding sites and exhibiting similar expression patterns between LNCaP and abl appear to maintain important metabolic gene expression profiles for both cell lines (Supplementary Table S2B) (13). This initial investigation of CREB1 in distinct models of prostate cancer suggests a broad and important role for this TF in determining cancer-relevant cell

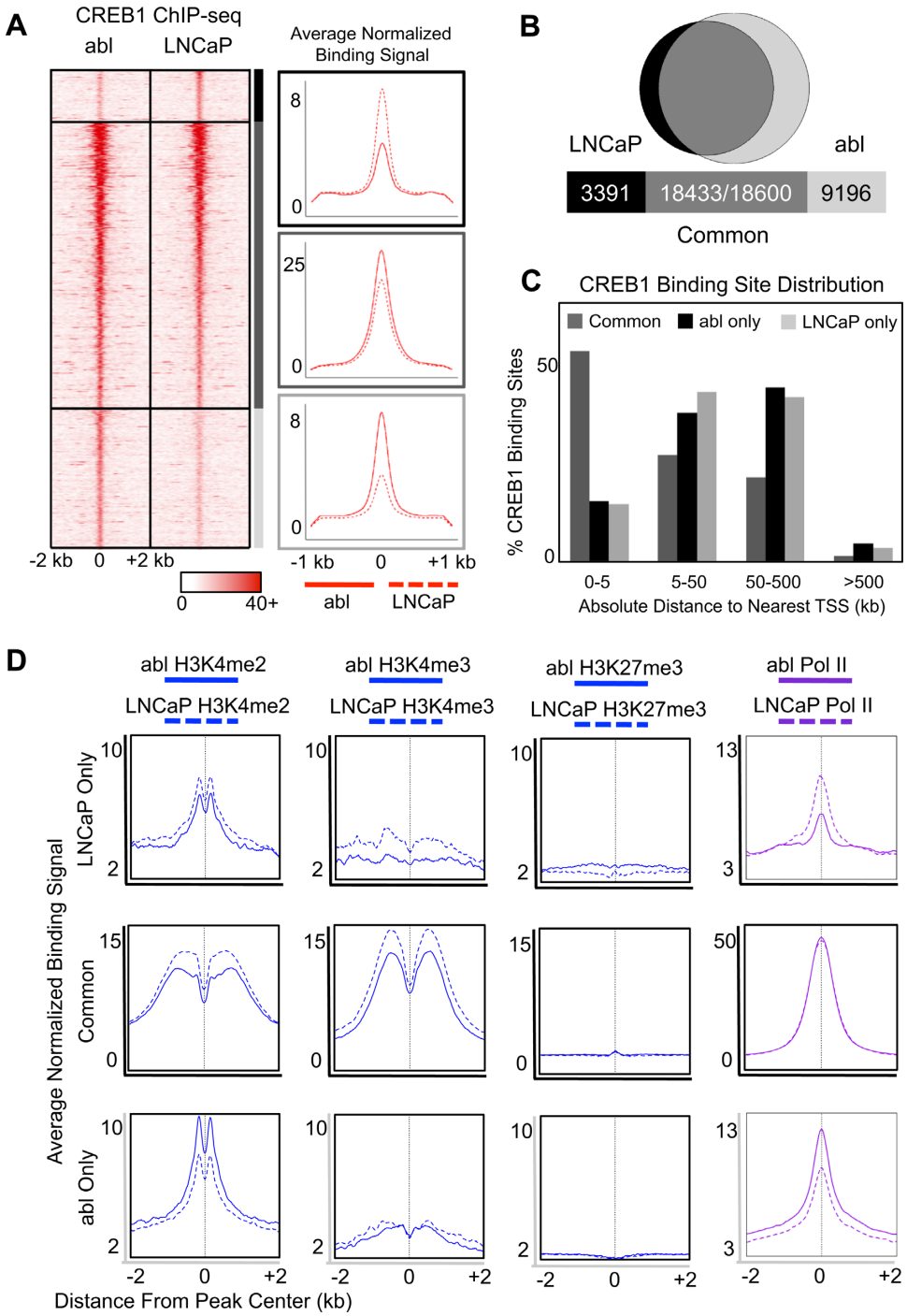

Figure 1. CREB1 ChIP-seq identifies cell type-specific enhancer binding. (**A**) Aligned reads heatmap of CREB1 ChIP-seq signal intensity centered over LNCaP-specific (black), common (dark gray) and abl-specific (light gray) CREB1 binding sites in descending order of peak strength within each category. Average signal plots for LNCaP and abl are provided (right) for each category. (**B**) Overlap of CREB1 peaks identified in LNCaP and abl cells. Common binding site numbers reflect the use of abl or LNCaP CREB1 peaks as bait. (**C**) Absolute distance to the nearest TSS was calculated for CREB1 binding sites in each category using the Genomic Regions Enrichment of Annotations Tool (GREAT). (**D**) Average signal plots for H3K4me2, H3K4me3, H3K27me3 (17,25), and Pol II (Z.C. and Q.W.) ChIP-seq assays in LNCaP and abl cells were plotted over CREB1 binding site categories.

cycle, pro-survival, and metabolic gene expression patterns via promoter as well as enhancer binding activity.

FoxA1 and CREB1 interact preferentially in CRPC cells

Recent investigations have documented the phenomenon of 'indirect peaks' identifiable in large-scale binding site data sets (28). This class of peaks are a newly appreciated result of the ChIP-seq protocol, which enriches not only the DNA fragments to which a TF is immediately bound through direct protein–DNA interactions, but also regions of the genome with which a TF may interact indirectly through scaffolding proteins involved in chromatin loop formation. Indirect peaks are generally characterized by lower affinity binding in comparison to direct peaks, and importantly, they lack the recognition motif that defines sequence-specific TF-DNA binding. As we identified relatively weak CREB1 binding in cell type-specific enhancer regions (Figure 1A), we next performed motif analysis to determine whether these regions satisfy both criteria for indirect peaks. Motif searching and *de novo* motif analysis of common and cell type-specific CREB1 binding sites identified previously reported Half- and Full-length cAMP response elements (CREs) (Figure 2A) (24,29). Specific enrichment of these relatively short motifs in all binding site categories was confirmed by motif scanning in CREB1 binding sites. Nearly all common CREB1 binding sites exhibited some version of the CRE (11%—Full CRE, 85% Half CRE) and high proportions of cell line-specific CREB1 binding sites also contained a CRE (LNCaP-specific: 8% Full CRE and 75% Half CRE, abl-specific: 7% Full CRE and 73% Half CRE). We also conducted scans for the Full and Half CREs in random genomic intervals matched to our three binding site categories and found that these motifs were significantly enriched in CREB1 binding sites compared to background (Supplementary Figure S2B). Together, these results suggest that CREB1 occupies distal enhancer regions in addition to proximal promoter regions via direct, sequence-specific DNA binding.

We also found the FoxA1 recognition motif among the most significantly enriched sequences in each CREB1 binding site category (Figure 2A), thus we performed FoxA1 ChIP-seq in LNCaP (19) and abl cells to characterize their genome-wide interaction (Supplementary Figure S2C). By plotting the FoxA1 ChIP-seq signal over CREB1 binding site categories, we get a picture of the extent to which these factors interact in both LNCaP and abl cells (Figure 2B). We found that abl FoxA1 peaks are significantly enriched compared to LNCaP FoxA1 peaks within abl CREB1 binding sites (both common and abl-specific). On the other hand, there was no significant enrichment of LNCaP FoxA1 binding events within LNCaP-specific CREB1 binding sites (Figure 2C). The preferential CREB1/FoxA1 interaction in CRPC cells was further supported by an inverse relationship between CREB1 and FoxA1 ChIP-seq signal intensity in LNCaP-specific CREB1 bound regions alone (Figure 2D). Large scale efforts aimed at unraveling complex transcription factor networks have previously revealed the context specificity with which such proteins interact to drive unique gene expression programs in various cancer models (30). Our results provide an interesting glimpse at such a phenomenon occurring in a model of disease progression within a single cancer type, and it will be of interest to elucidate which of the many candidate TFs identified by motif searching preferentially interact with CREB1 in the ADPC context (Supplementary Figure S2D).

CREB1/FoxA1 co-regulatory activity

We then sought to understand how differences in the spatial overlap of CREB1 and FoxA1 in abl compared to LNCaP cells impacts on their functional overlap in defining gene expression profiles. We performed RNA-seq in LNCaP and abl cells following FoxA1 silencing for inclusion in our analysis. We then employed a global target gene identification approach for CREB1 and FoxA1, which acknowledges functional promoter and/or enhancer binding of each TF near potential target genes. Integrating binding site and gene expression profiles from LNCaP and abl cells, we identified genes ±50 kb from all CREB1 and FoxA1 binding sites in LNCaP and abl cells. We filtered the resulting gene lists based on responsiveness to siCREB1 or siFoxA1 transfection, respectively (edgeR: $\geq$ 1.2-fold change compared to siControl, P-value < 0.05, and false discover rate (FDR) $< 5\%$). Figure 2E reports the number of CREB1- and FoxA1-responsive genes identified as well as the degree of overlap between CREB1- and FoxA1-regulated genes in LNCaP versus abl cells. Consistent with the heightened physical overlap of CREB1 and FoxA1 binding sites in abl cells, these TFs appear to co-regulate a much larger set of common transcriptional targets in abl cells compared with LNCaP cells (cumulatively 4117 and 1867 up/downregulated genes in abl and LNCaP, respectively) (Figure 2F and Supplementary Table S2C). A complementary target gene identification approach (see 'Materials and Methods' section) (31) revealed that CREB1/FoxA1 co-regulated genes in LNCaP cells were preferentially driven by non-overlapping CREB1 and FoxA1 binding events, while CREB1/FoxA1 target genes in abl cells were specifically enriched with overlapping TF binding sites (Supplementary Figure S3A). While the complementary approach was useful in revealing this intriguing aspect of cooperative TF activity and identified 100% of the co-regulated genes found from our initial target gene identification approach, it was less conservative overall. Gene ontology analysis revealed that cooperative CREB1/FoxA1 transcriptional activity likely supports important, disease-driving expression profiles in both ADPC and CRPC cells. For example, in abl cells, CREB1/FoxA1 enhance cell cycle, more specifically mitotic, signaling while repressing differentiation programs (Figure 2G and Supplementary Table S2D).

Complex hierarchy characterizes CREB1–FoxA1 interaction

As CREB1 and FoxA1 have been widely regarded as promoter- and enhancer-binding factors, respectively, it was intriguing to reveal the breadth of their physical interaction in CRPC cells, and we wondered if these factors might influence each other's binding patterns. We have previously explored the hierarchical nature of CREB1 and FoxA1 binding near a small number of genes in abl cells (10), but we sought to define this relationship at the genome-wide level. To this end, we conducted CREB1 ChIP-seq

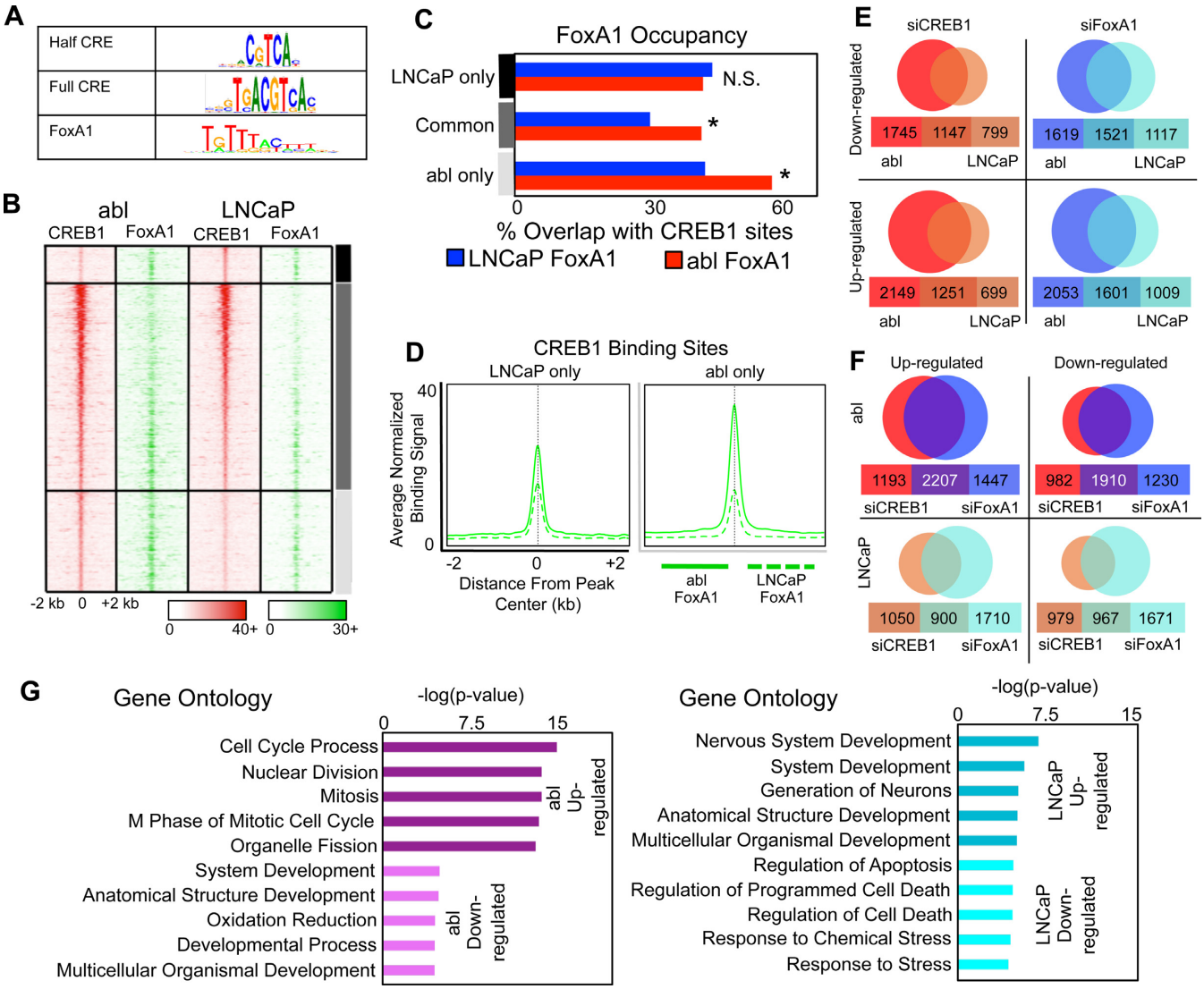

Figure 2. Extensive CREB1/FoxA1 co-regulatory activity in ADPC and CRPC cells. (**A**) Motif analysis of CREB1 binding site categories. (**B**) Heatmap of FoxA1 ChIP-seq signal over CREB1 binding sites ordered as in Figure 1A. (**C**) FoxA1 peak overlap with CREB1 binding site categories in LNCaP and abl cells (Fisher's exact test—* indicates P-value $< 10^{-5}$, N.S. = not significant). (**D**) LNCaP and abl FoxA1 ChIP-seq average signal is plotted over cell type-specific CREB1 binding sites. (**E**) GREAT was used to identify genes ±50 kb from all CREB1 or FoxA1 binding sites in LNCaP and abl cells. Resulting lists were filtered based on response of each gene to siCREB1 or siFoxA1 transfection compared to siControl transfection in LNCaP and abl cells measured by RNA-seq ([Fold Change] ≥ 1.2, P-value ≤ 0.05, FDR $\leq 5\%$). siCREB1 and siFoxA1 up- and downregulated gene lists from LNCaP and abl cells were overlapped. (**F**) Overlap of siCREB1- and siFoxA1-responsive genes from each cell line. (**G**) Gene ontology analysis of putative CREB1/FoxA1 co-regulated genes in LNCaP versus abl cells (complete list in Supplementary Table S2D).

in abl cells following siControl or siFoxA1 transfection as well as FoxA1 ChIP-seq following siControl or siCREB1 transfection (Supplementary Figure S3B). We found that a small minority of FoxA1 binding sites (3531/61 423) was lost upon CREB1 silencing (Figure 3A). Though just 10% of these sites overlapped with CREB1 peaks, we were able to find the CREB1 sequence motif within this category of siControl-specific FoxA1 binding sites, suggesting some small level of direct CREB1 influence on FoxA1 binding. While we observed a striking gain of 16 196 siCREB1-specific FoxA1 binding sites primarily outside of promoter regions, only 8.3% of these regions were occupied by CREB1 under siControl conditions, and motif analysis failed to discover the CREB1 binding motif in this FoxA1 binding site category. We validated a set of siControl- and siCREB1-specific FoxA1 binding sites by standard ChIP-qPCR and found that this remarkable influence of CREB1 over FoxA1 binding patterns was robust and reproducible (Supplementary Figure S3C). Similar patterns were observed in our analysis of CREB1 ChIP-seq data (Figure 3B). Approximately 20% of CREB1 sites were lost upon FoxA1 silencing. These sites existed primarily outside of promoter regions, overlapped considerably with FoxA1 binding sites, and were highly enriched for the FoxA1 binding motif. In contrast, CREB1 binding sites that were gained upon FoxA1 silencing occurred more frequently within promoters, did not overlap with FoxA1 binding sites and were depleted of the FoxA1 motif.

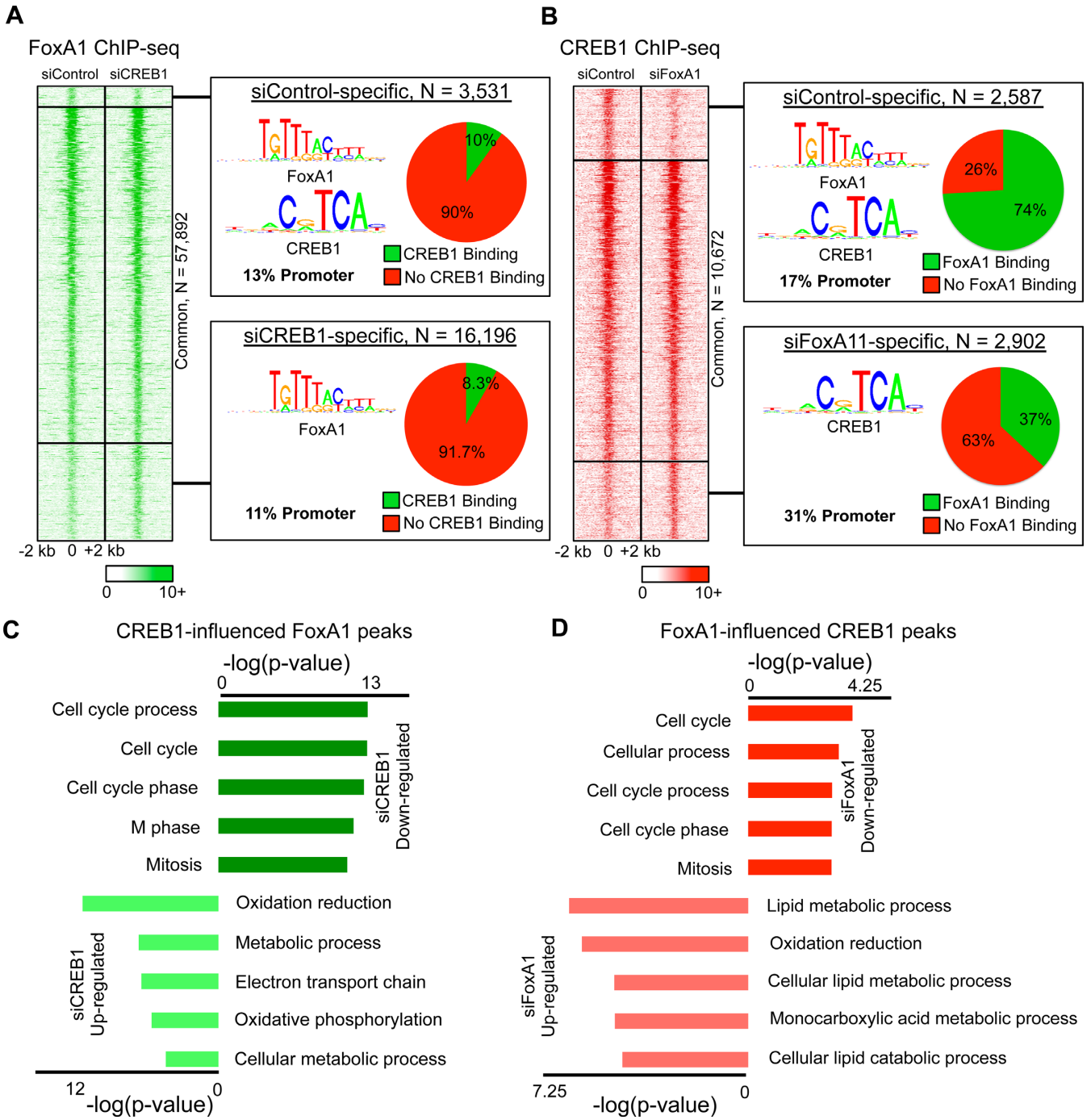

Figure 3. Genome-wide analysis of CREB1/FoxA1 hierarchical binding in CRPC cells. (**A**) Heatmap of FoxA1 ChIP-seq signal intensity over siControl-specific, common and siCREB1-specific FoxA1 binding sites. Boxes to the right display binding site numbers, motif occurrences, promoter occupancy and overlap of CREB1 binding with siControl and siCREB1 specific FoxA1 binding sites. (**B**) Heatmap of CREB1 ChIP-seq signal intensity over siControl-specific, Common and siFoxA1-specific CREB1 binding sites. Boxes to the right display binding site numbers, motif occurrences, promoter occupancy and overlap of FoxA1 binding with siControl and siFoxA1 specific CREB1 binding sites. (C-D) Gene ontology analysis of genes ±50 kb from CREB1-influenced FoxA1 (**C**) and FoxA1-influenced CREB1 (**D**) binding sites that were responsive to CREB1 or FoxA1 silencing, respectively.

Altogether, these observations demonstrate that while the vast majority of CREB1 and FoxA1 binding sites occur independently of the other factor, subsets of each factor's cistrome are influenced both positively and negatively by the direct as well as indirect actions of the other factor. Our group and others have similarly explored the effect of cooperative transcription factors upon one another as they co-localize to common genomic regions (19,32). These investigations have generally revealed unidirectional patterns of influence in which the binding of pioneer factors like FoxA1 appear unaffected by the loss of their binding partners. Other works have also noted the high prevalence of *trans* binding repression observed here (33), wherein silencing of one binding partner allows for new binding of the second partner in regions unoccupied by either factor under standard conditions. It is interesting to note that *trans* repression was the primary manner in which CREB1 influenced FoxA1 binding in abl cells (Figure 3A). Consistent with a previous study of the impact of FoxA1 silencing on AR genomic binding patterns (33), FoxA1 exerts both *cis* recruitment and *trans* repressive influence over CREB1 binding (Figure 3B). Our current investigation suggests that complex relationships exist between factors whose functional overlap in defining gene expression programs may be more profound than the physical overlap in their binding patterns, as appears to be the case for CREB1 and FoxA1. To provide further support for the notion of a functional CREB1/FoxA1 overlap resulting from their mutual impact on each other's binding patterns, we identified genes regulated by FoxA1-influenced CREB1 binding sites (either lost or gained) and CREB1-influenced FoxA1 binding sites using our integrated target gene identification approach. This revealed nearly absolute concordance in the pathways influenced by the complex hierarchical relationship between CREB1 and FoxA1 (Figure 3C and D).

CREB1/FoxA1 target genes associated with recurrent prostate cancer

Having revealed that the CREB1/FoxA1 target genes identified in LNCaP and abl cells are enriched within disease-relevant biological processes, we next asked if these genes were associated with human prostate cancer progression. CREB1/FoxA1 up- and downregulated genes (Supplementary Table S2C) were uploaded for ONCOMINE Concept Analysis (34) to assess their enrichment in gene sets whose differential expression characterizes diverse patient cohorts of varying disease severity. We found that CREB1/FoxA1 target genes were highly enriched in numerous ONCOMINE Concepts, and that targets identified in LNCaP and abl cells mapped almost entirely to non-overlapping concepts (Figure 4A and Supplementary Table S2E). For example LNCaP upregulated targets were among the top 5% overexpressed genes in cancer versus normal prostate tissue as measured in a study by Taylor *et al.* (6), while abl upregulated genes were among the top 1% overexpressed genes in patients from the same study who had recurrent disease within 5 years after prostatectomy.

Prioritizing genes that were common to multiple ONCOMINE Concepts and therefore broadly characteristic of diverse patient populations, we then refined our large lists of CREB1/FoxA1 target genes identified in LNCaP and abl cells (see 'Materials and Methods' section) to arrive at two gene panels we hypothesized would correlate with poor outcomes: the 19-gene Panel A (CREB1/FoxA1 upregulated genes identified in abl cells: *TPX2, CDKN3, BUB1, TOP2A, NCAPG, UBE2C, PLK1, ASPM, CENPF, C15orf42, KIF4A, PBK, NUSAP1, HMMR, CIT, ANLN, SKA3, BIRC5, PRC1*) and the 6-gene Panel B (CREB1/FoxA1 downregulated genes identified in abl cells: *AZGP1, CRISPLD2, EPHX2, HSPB8, PTRF, MFGE8*). For analysis of the prognostic/predictive power of our final gene panels, we selected two cohorts with published gene expression microarray data in primary prostate cancer tissue from relatively large cohorts of mainly low and intermediate risk patients: Taylor *et al.* and Glinsky *et al.* (22). These studies include extensive clinical information for each patient including median follow-up $\geq$5 years, and importantly, these studies were the only two identified that measured a majority of our panel genes (exceptions being the absence of data for *C15orf42, ANLN,* and *SKA3* in the Glinsky cohort). Kaplan–Meier survival analysis demonstrated that high expression of Panel A and low expression of Panel B correlated strongly with shorter time to biochemical recurrence in the Taylor and Glinsky cohorts (Figure 4B) (22). We were unable to assemble any such prognostic gene panel from LNCaP CREB1/FoxA1 target genes. To address the possibility that expression patterns of Panel A and B genes generally correspond with poor outcomes in solid malignancies rather than characterizing prostate cancer outcomes specifically, we used cBioPortal (23) to perform survival analysis in several additional cancers and found that these gene panels do not appear to relate to shorter overall survival (breast, colorectal, head and neck, and lung) or disease-free survival (ovarian) (Supplementary Figure S4) (35,36). By simulating the selection of 2000 random 19- and 6-gene sets, we found that the probabilities of randomly arriving at similarly predictive gene panels (i.e. having log-rank *P*-values in the Taylor cohort of 5.3×10^{-4} and 0.0022, respectively) were just 0.0015 and 0.025 for Panel A and Panel B, respectively.

Ontology analysis of Panel A genes revealed that this cohort of CREB1/FoxA1 targets are primarily responsible for enhancing mitotic cell cycle. This supports our previous findings that both G1/S and G2/M phase progression are mediated in part by cooperative CREB1/FoxA1 transcriptional activation (involving our previously described Panel A member, *UBE2C*) (10,15–16). Interestingly, our Panel A genes overlap considerably (10 out of 19) with a 31-gene panel used to develop a cell cycle progression score for determining risk of biochemical recurrence (37). Additionally, *CENPF*, recently reported as a top-tier driver of advanced prostate cancer is also present in our panel (38). Together, these data support the concept that enhanced cell cycle gene expression patterns are a hallmark of aggressive prostate cancer. That multiple investigations have arrived at such findings and have demonstrated the ability to predict subsequent recurrence using cell cycle gene expression profiles of primary prostate cancer tissue suggests further development of these panels would be of definite clinical utility.

Panel B genes, are largely absent from reported prostate cancer prognostic gene panels. A notable exception is

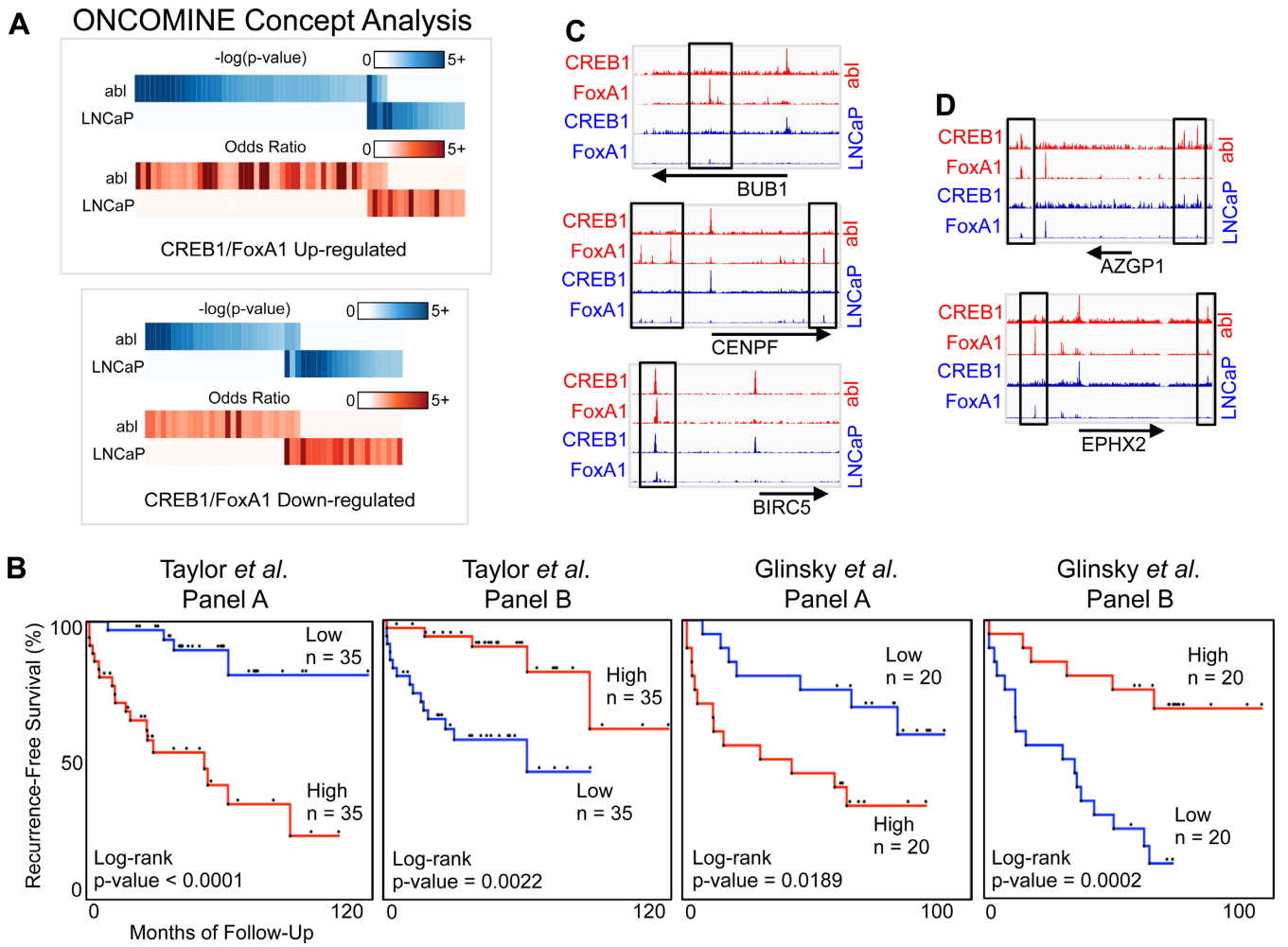

Figure 4. Defining predictive CREB1/FoxA1 co-regulated gene panels. (**A**) ONCOMINE Concept Analysis of CREB1/FoxA1 co-regulated genes in LNCaP versus abl cells. *P*-value/odds ratio for ONCOMINE Concept enrichment is provided for each gene category (see Supplementary Table S2E for Concept names). (**B**) Kaplan–Meier curves comparing recurrence free survival of two patient cohorts (Taylor *et al.* and Glinsky *et al.*) distinguished by low (bottom quartile) versus high (top quartile) expression of Panel A or Panel B genes. (**C** and **D**) IGV plots of CREB1 and FoxA1 ChIP-seq signal over example Panel A (C) and Panel B (D) gene loci. Vertical scales are the same for each factor between cell lines.

AZGP1, which can be found among the genes measured in the Oncotype DX® Prostate Cancer Assay used to more accurately stratify clinical disease risk and has been reported previously as a prostate tumor suppressor (39,40). Tumor suppressive functions of additional Panel B genes have also been reported. In prostate cancer models, restored *PTRF* expression was shown to diminish angiogenesis and metastatic potential (41,42). Additionally, reversal of DNA methylation-dependent *HSPB8* silencing in prostate cancer cells induced apoptosis (43). Other Panel B genes appear to have more complex functionality. In breast cancer models, *MFGE8* may serve as a tumor suppressor in ER+/HER2+ cells, while its silencing in triple negative cells results in enhanced sensitivity to DNA crosslinking chemotherapy (44). *EPHX2* has been reported as a putative tumor suppressor in breast cancer, though its role as a potent oncogene, corresponding to AR-mediated signaling, has also been reported in prostate cancer (45–47). Finally, while its related CAP protein family member *CRISP3* exhibits enhanced expression in prostate cancer compared to normal tissue, suggesting its role as an oncogene in primary cancer, no such report was found for *CRISPLD2* (47).

We found that the recently reported TUSON model predicted essentially no oncogenic or tumor suppressor function for any of our Panel A or B genes, respectively, in either a cross-cancer or prostate cancer-specific analysis, which is based on higher than expected genetic alteration rates in cancer versus normal tissue (48). This finding suggests that transcription regulation mediated by CREB1/FoxA1 activity, rather than mutation, could provide a means of oncogene activation and tumor suppressor loss in advanced prostate cancer. Additional inspection of mutation data from six prostate cancer cohorts using cBioPortal revealed extremely low mutation rates for Panel A and Panel B genes; *ASPM* was the most frequently mutated, exhibiting entirely discrete alterations in 1.54% of the 972 patients analyzed across all cohorts. This further supports the notion that our genes panels represent so-called 'epi-driver genes,' which are distinguishable from commonly mutated cancer drivers and

characterized by abnormal expression patterns in cancerous tissue (49).

To understand the basis for their deregulated expression from a mechanistic perspective, closer inspection of the CREB1 and FoxA1 occupancy at Panel A gene loci revealed that while CREB1 binding remains relatively constant at Panel A promoters between ADPC and CRPC cells, FoxA1 accumulation in distal enhancer regions specifically in abl cells corresponds with their overexpression in this cell type (Figure 4C and Supplementary Figure S5A). Around Panel B genes, we found several examples of abl-specific CREB1 and/or FoxA1 binding sites in the distal regulatory regions of Panel B genes (Figure 4D and Supplementary Figure S5B). This indicates a potential disruption of Panel B gene maintenance in CRPC cells via disease stage-specific, CREB1/FoxA1 enhancer binding. Reviewing the siCREB1/siFoxA1 ChIP-seq data, we found examples of CREB1-*trans*-repressed FoxA1 binding sites near *NCAPG*, *C15orf42*, *PBK*, *HMMR*, *CIT* and *MFGE8* as well as a FoxA1-*cis*-recruited CREB1 binding site near *AZGP1*, further demonstrating these predominant modes of mutual influence between CREB1 and FoxA1 within our gene panels.

CREB1/FoxA1 co-regulated genes predict prostate cancer recurrence

At this point, we performed clustering analysis of patients in the Taylor and Glinsky cohorts to determine whether Panel A and Panel B gene expression levels could identify distinct patient subsets (Figure 5A and B). Indeed, highly contrasting clusters emerged within each cohort. Notably, the clusters marked by orange and red bars in each cohort, representing strong expression of Panel A and weak expression of Panel B genes, capture a larger proportion of patients with a biochemical recurrence event after prostatectomy (Taylor = 24/36, Glinsky = 24/37) than the green cluster representing the opposite gene expression pattern (Taylor = 7/36, Glinsky = 12/37) (Fisher's Exact: Taylor *P*-value = 0.0001, Glinsky *P*-value = 0.01). We also noted that values for serum prostate-specific antigen (PSA) concentration at prostatectomy and Gleason Score differed significantly between the Glinsky and Taylor cohorts (annotated along the top of Figure 5A and B) (PSA—Mann–Whitney U *P*-value = 0.003, Gleason—Pearson χ^2 *P*-value < 0.0001), thus we chose to pool these patients into a combined cohort to more accurately represent a broader population for subsequent analyses.

We hypothesized that expression patterns of Panel A and B genes might combine with clinical features to add prognostic value when predicting risk of prostate cancer outcomes, and we first assessed whether Panel A and B levels were independent of PSA, Gleason Score and Stage in our combined cohort. We found that Panel B was statistically correlated with Gleason Score alone, and similarly, Panel A was only correlated with a change in Gleason from 7 to above 7 (Supplementary Table S3A). In general, these results were recapitulated in analyses of the Taylor and Glinsky cohorts individually (Supplementary Table S3B and C). Together these results suggested that Panel A and Panel B genes were indeed largely independent of clinical prognosticators, and thus had the potential to provide valuable new information to statistical models of progression. We next performed univariate Cox regression analysis for Gleason, PSA, Stage and both Panel A (Hazard Ratio (HR) = 1.40, 95% Confidence Interval (CI) = 1.21–1.58) and Panel B (HR = 0.56, 95% CI = 0.47–0.67) in the combined cohort, finding that each parameter was highly significant in predicting earlier biochemical recurrence (Supplementary Table S4A). In a multivariate model of clinical features alone, Gleason, PSA and Stage were all significant model parameters (Supplementary Table S4B), and when Panel A or Panel B was added to generate a combined clinical/molecular model, all parameters remained highly significant (Supplementary Table S4C and D). While our panel assembly method selected for within-panel correlation in gene expression patterns, we also found that there was significant between-panel correlation (Spearman's ρ *P*-value < 0.0001, Supplementary Table S3A and C) that suggests our panels may be partially redundant to one another. Concordantly, when we assembled a proportional hazards model including clinical features and both gene panels, individual gene panel effect sizes were reduced or, in the case of Panel A, became only marginally significant (Supplementary Table S4E). As with our earlier correlation analyses, proportional hazards modeling in the individual Taylor and Glinsky cohorts largely reflected our analysis of the combined cohort (Supplementary Table S4F–O), including the reduction in effect size of each gene panel when considered in combination alongside clinical features. Regarding Panel A, this data supports previous associations of cell cycle gene expression levels with prostate cancer recurrence, showing that this functional gene set adds significant value to prognostic models based on clinical features. On the other hand, our Panel B analysis stands alone in showing that lowered expression of this set of putative tumor suppressors corresponds with more rapid prostate cancer recurrence.

We also asked if our gene panels might be utilized in a logistic regression analysis for the prospective, binary classification of patients who will or will not experience a biochemical recurrence event. Utilizing the combined cohort, univariate analysis showed that PSA, Stage, Gleason, Panel A and Panel B could all be used to classify patients by predicted recurrence, with Gleason score being the strongest clinical predictor as assessed by the receiver operating characteristic (ROC) curve (area under the curve (AUC) = 0.738) and Panel A and B performing similarly (AUC = 0.683 and 0.710, respectively) (Supplementary Figure S6A). As in our proportional hazards model, when Panel A and Panel B were considered in combination, Panel A became only marginally significant, though the model itself outperformed individual gene panel models (AUC = 0.722). In a multivariate clinical model, PSA, Stage and Gleason were all significant model parameters, outperforming the best univariate models (AUC = 0.784) (Supplementary Figure S6B). In combined clinical/molecular multivariate models, we found that the addition of Panel A, Panel B, or both Panel A and B improved upon the clinical-only model (AUC = 0.821, 0.810 and 0.822, respectively). To better understand how our gene panels were able to improve the accuracy of these recurrence prediction models, we needed to validate each model's performance in an independent cohort. To this end, we randomly divided the

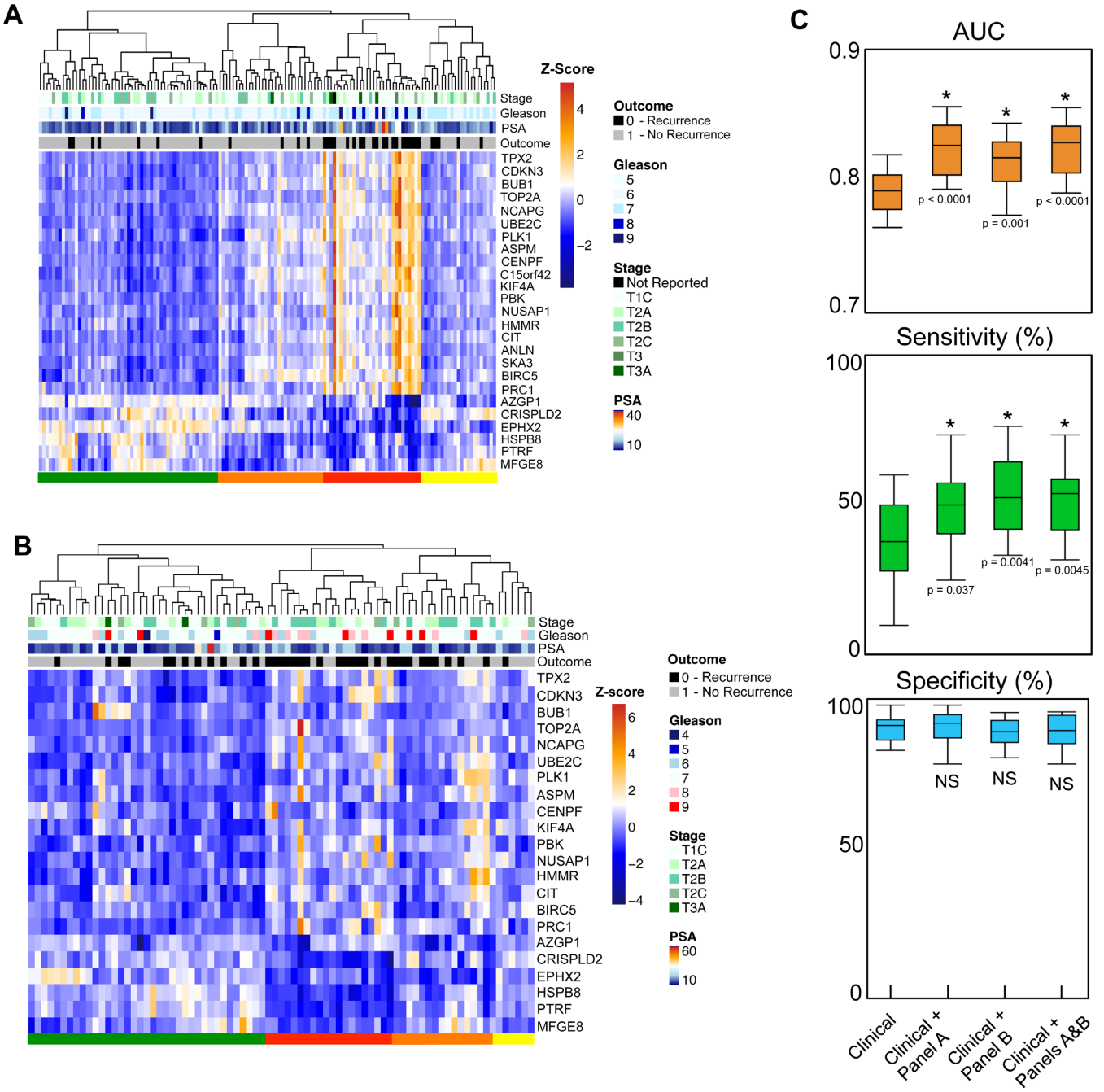

Figure 5. CREB1/FoxA1-regulated gene panels predict prostate cancer recurrence. (**A**) Taylor cohort was clustered (Pearson correlation) by Panel A and Panel B expression. Clinical information is annotated along the top of the figure. (B) Glinsky cohort was clustered as in (A). Clinical information is plotted along the top of the figure. (**C**) Logistic regression models ($n = 20$ for each combination of model parameters) were trained on a random 75% of the combined cohort and validated on the remaining 25%. AUC, Specificity and Sensitivity values for each model are displayed as box plots. Significant difference assessed by Mann–Whitney U with $\alpha = 0.0083$ to correct for multiple comparisons (*—Significant (*P*-value displayed), NS—Not Significant).

combined cohort into a training subset representing 75% of the total cohort, and a validation subset representing the remaining 25%. The training subset was utilized to generate logistic regression models for clinical features alone or in combination with Panel A and/or Panel B. The coefficients of each model were then applied to the validation subset, and the process was repeated 20 times. As in our analysis of the entire combined cohort, we found that the AUC metric improved significantly upon inclusion of molecular information to existing clinical prognosticators (Figure 5C). Assessing the performance of these models in the validation cohorts, we determined that this improvement could be attributed to an increase in model sensitivity, while our gene panels did not significantly impact model specificity. This important outcome demonstrates that our newly defined, independent molecular features are capable of identifying

at-risk patients not captured by current clinical prognosticators without an increase in false positives.

To find if our gene panels also correlated with a second clinical outcome, the development of resistance to hormone therapy, we conducted an analysis of Panel A and Panel B gene expression in circulating tumor cells (CTCs) isolated from a cohort of prostate cancer patients who had received hormone therapy for metastatic or recurrent disease. In this nested study, we measured an average of 12 CTCs from 10 patients whose disease remained sensitive to therapy (CS) and 15 patients who had developed resistance (CR) as indicated by rising serum PSA concentration (Supplementary Figure S7A and Supplementary Table S1B). Panel B genes were often significantly under-expressed in CR compared to CS patient-derived CTCs (Supplementary Figure S7B), though this trend was not maintained at the patient level. We observed much more similar expression patterns of Panel A genes in CTCs isolated from CR versus CS patients (Supplementary Figure S7C), and again found no between-patient differences in Panel A expression levels. Though our sample size was small, these results suggest that the primary value of our gene panels is in predicting recurrence among primary prostate cancer patients, and that they may not further distinguish patients who have or will develop treatment resistance among a population of recurrent prostate cancer patients in which gene panel expression changes have likely already occurred.

Disrupting CREB1/FoxA1 target gene expression via phospho-MED1 inhibition

We finally explored a strategy to target CREB1/FoxA1 signaling in advanced prostate cancer cell lines. Though its basal transcriptional activity can occur in the absence of an activating phosphorylation event at serine 133 (Ser133), CREB1 signaling presents an attractive therapeutic target as this TF's transactivation potential is dramatically enhanced by druggable kinases including PKA (13,14). Ser133-phosphorylated-CREB1 (pCREB1) has been proposed as a potential prostate cancer biomarker (50), with increased pCREB1 levels correlating with more aggressive disease, and several studies have explored the use of various kinase inhibitors to abrogate, for example, parathyroid hormone- or epidermal growth factor-stimulated CREB1 (51). We set out to inhibit endogenous CREB1 or pCREB1 activity in the absence of external stimuli.

We conducted our initial analysis in 22rv1 cells, as these exhibited similar protein expression but much stronger phosphorylation of CREB1 compared to abl, C4–2B and PC-3 cell lines (Supplementary Figure S8A). Fourteen of our Panel A genes, which were significantly over-expressed in abl compared to LNCaP cells, were further upregulated in 22rv1 cells and we selected eight Panel A genes (*ASPM*, *CENPF*, *CIT*, *HMMR*, *PBK*, *PRC1*, *SKA3* and *UBE2C*) and four of our previously identified CREB1/FoxA1 target genes (*CCNA2*, *CCNE2*, *E2F1* and *CDK1*) (10) for further analysis (Supplementary Figure S8B). Standard ChIP-qPCR assays revealed nearly identical binding of CREB1 to the promoter regions of all 12 genes in abl and 22rv1 cells (Supplementary Figure S8C). Ser133 phosphorylation in the CREB1 KID domain generates a substrate for histone acetyltransferase CBP/p300 recruitment (52), thus we observed significantly higher enrichment of both CBP and p300 as well as enhanced histone H3 lysine 27 acetylation (H3K27ac) levels at all gene promoters in 22rv1 compared to abl cells (Supplementary Figure S8C). Enhanced transcriptional activity was also indicated by higher RNA polymerase II (Pol II) recruitment to 10/12 gene promoters in 22rv1 cells (Supplementary Figure S8C). Consistent with the role of the Mediator co-regulatory complex subunit MED1 in forming transcription regulatory chromatin loops between enhancer- and promoter-bound transcription factor complexes (i.e. FoxA1 and CREB1, respectively) (15), we also observed binding of threonine 1032–phosphorylated MED1 (pMED1) at all gene promoters in abl cells, and found significantly enhanced pMED1 occupancy in 22rv1 cells (Supplementary Figure S8C).

Though the kinase inhibitor H89 has been used extensively to study and target CREB1 activity enhanced by stimuli such as forskolin, we found that H89 treatment alone could not reliably reduce endogenous pCREB1 levels in 22rv1 cells (Figure 6A). Paradoxically, 22rv1 cells exhibited a dose-dependent reduction in CREB1/FoxA1 target gene expression in response to H89 treatment (Figure 6B). These results suggest that H89 has some impact on CREB1/FoxA1 signaling without directly affecting CREB1 *per se*. This notion was supported by the maintenance of CREB1 as well as CBP and p300 recruitment to target gene promoters following H89 treatment (Figure 6C). We hypothesized that H89 may have some effect on the modification/activity of other CREB1/FoxA1 co-regulators and were intrigued to find that pMED1 but not total MED1 expression levels were dramatically reduced by H89 treatment (Figure 6A). pMED1 binding to target gene promoters was also attenuated by H89 treatment, which corresponded to Pol II destabilization across most genes (Figure 6C). This is consistent with another known role of the Mediator complex in establishing and maintaining the stability of the pre-initiation complex (PIC) at Pol II-transcribed genes promoters (53).

To help verify our results, we sought to reproduce our findings by inhibiting known MED1 kinases, Akt and Erk (15,54). As 22rv1 cells are PTEN wild-type and exhibit very low levels of phosphorylated Akt (Supplementary Figure S8D), the Akt inhibitor MK-2206 was not effective in diminishing CREB1/FoxA1 target gene expression in 22rv1 cells (Supplementary Figure S8E). Treatment with the MEK inhibitor U0126 reduced Erk phosphorylation and recapitulated the results of H89 treatment, including reduced pMED1 levels, CREB1/FoxA1 target gene expression and pMED1 and Pol II recruitment to promoters (Figure 6D–F). As this treatment strategy appears not to act directly via inhibition of CREB1 phosphorylation, we hypothesized that it would remain effective in cells with low endogenous pCREB1 levels. Concordantly, abl cells exhibited dramatically reduced CREB1/FoxA1 target gene expression levels following H89 and U0126 treatment (Supplementary Figure S8F). Additionally, as abl cells have activated Akt (Supplementary Figure S8D), we found that this signaling axis was also sensitive to MK-2206 treatment in abl cells (Supplementary Figure S8F). We then asked if these kinase inhibitors, which impact broad-ranging cellu-

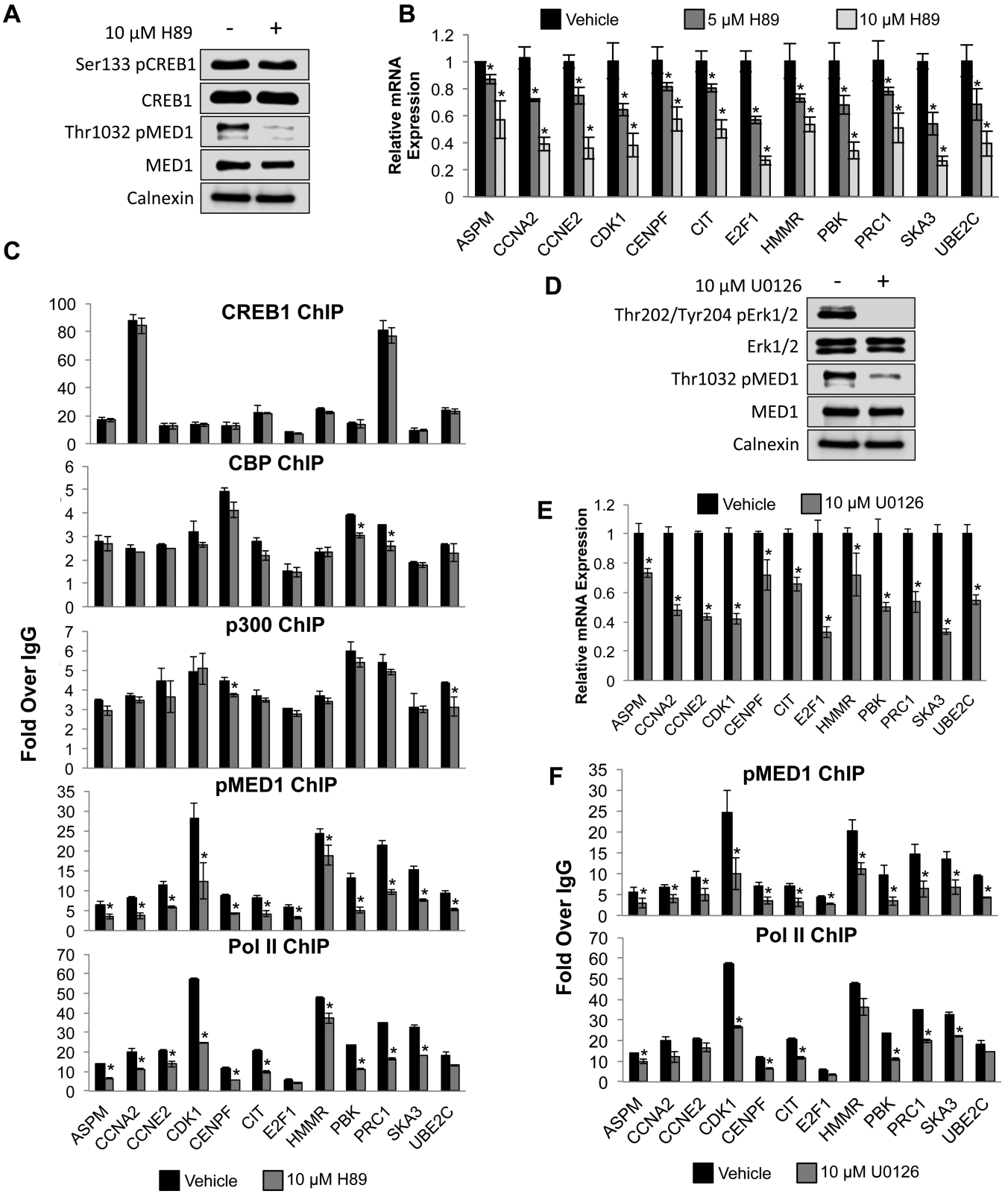

Figure 6. Kinase inhibition of CREB1/FoxA1 transcriptional activity. (**A**) Representative western blot of 22rv1 cells treated for 24 h with vehicle or H89. (**B**) CREB1/FoxA1 target gene expression was measured by qRT-PCR in 22rv1 cells treated for 24 h with vehicle or H89 ($n = 3$–4). (**C**) ChIP-qPCR was conducted at the promoters of CREB1/FoxA1 target genes using the indicated antibodies in 22rv1 cells treated for 24 h with vehicle or H89 ($n = 2$). (**D**) Representative western blot of 22rv1 cells treated for 24 h with vehicle or U0126. (**E**) CREB1/FoxA1 target gene expression was measured by qRT-PCR in 22rv1 cells treated for 24 h with vehicle or U0126 ($n = 3$–4). (**F**) ChIP-qPCR was conducted at the promoters of CREB1/FoxA1 target genes using the indicated antibodies in 22rv1 cells treated for 24 h with vehicle or H89 ($n = 2$). * Indicates significant P-value < 0.05, two-sided Student's t-test.

lar processes, exhibit similar transcription inhibitory activity over non-CREB1/FoxA1 targets. We selected 10 genes that failed to meet either criteria of a target gene (TF binding and TF-responsive expression) but were still highly expressed in our RNA-seq data. These genes were largely unaffected, and in some cases induced, by all compounds tested in both 22rv1 and abl cells (Supplementary Figure S9A), suggesting that the CREB1/FoxA1 axis is a prominent target of their chemical activity.

AR has been shown to play at least a partial role in supporting the expression of several of our CREB1/FoxA1 target and Panel A genes (10). Additionally, Hu *et al.* reported that forced expression of the constitutively active AR V7 splice variant in LNCaP cells caused the upregulation of several Panel A genes in the absence of hormone (55). This presents a potential confounding factor in 22rv1 cells, which express both full-length AR (AR FL) as well as AR splice variants (AR Vs) (Supplementary Figure S9B). To assess whether CREB1/FoxA1 target gene expression is driven by AR activity in this model, we transfected 22rv1 cells with AR-targeting siRNA and measured the expression of *PSA* as well as our CREB1/FoxA1 target genes (Supplementary Figure S9C-D). While *PSA* expression after AR knockdown dropped to <50% of control, expression of reported AR-regulated genes that we identified here as CREB1/FoxA1 targets (*CCNA2, UBE2C, CDK1*) (10,16,56) was only marginally, though significantly inhibited by AR knockdown, and other CREB1/FoxA1 targets were entirely unaffected (Supplementary Figure S9D). We therefore suggest that AR plays only a minor role in supporting the expression of these genes in certain cellular contexts.

Together, our results reveal that prostate cancer-driving CREB1/FoxA1 transcriptional activity is sensitive to broad inhibition of the indispensible co-activator MED1. Additionally, these results provide an interesting example of how CREB1 transcriptional activity can be altered in the absence of any apparent effect on its phosphorylation (14).

DISCUSSION

Our analysis has provided several intriguing outcomes and a functional view of how transcription factor networks acting outside the androgen/AR signaling axis contribute to prostate cancer growth and progression. This study enhances the growing body of research defining CREB1 as an important driver of various cancers including leukemia, non-small cell lung cancer, breast cancer and prostate cancer (57–59), and encourages continued development of novel CREB1-inhibiting compounds that either affect kinase-dependent CREB1 transactivation or impinge upon its relationship with collaborators/co-regulators such as FoxA1 and MED1 (60). Our integrative genomics approach identified CREB1/FoxA1 activity as a targetable signaling axis defining the expression of prognostic/predictive biomarkers for primary prostate cancer, in which the discovery of clinically actionable genetic alterations has been challenging.

While prognostic gene signatures that aid in the difficult task of stratifying risk in prostate cancer patients continue to emerge, the mechanism of their deregulated expression is often not addressed, leaving the extent of their clinical utility partially untapped (37,61). We found that CREB1/FoxA1 signaling assumes direct regulatory control over a large proportion of genes that were assembled in developing a prognostic, cell cycle progression score reported previously (10/19 Panel A genes) (37). While some overlap between these cell cycle genes and CREB1/FoxA1 co-regulated genes could be expected based on our knowledge that these TFs regulate both G1/S (*CCNE2, CCNA2,* and *E2F1*) and G2/M (*UBE2C* and *CDK1*) phase gene expression (10), the more than 50% overlap provides evidence for the central role of CREB1 and FoxA1 in driving a disease-relevant cell cycle gene expression program associated with poor clinical outcomes. The fact that Panel A is enriched within commonly over-expressed genes among aggressive prostate cancers (Figure 4A), further suggests that enhanced cell cycle signaling is a hallmark of advanced disease. Thus, our findings provide additional justification for developing predictive and prognostic tools based on cell cycle signaling downstream of CREB1/FoxA1, and we further suggest that prostate cancer patients characterized by heightened cell cycle signaling might be inherently sensitive to CREB1/FoxA1 inhibition.

Our analysis also revealed a small set of known as well as potential tumor suppressors, inactivated by CREB1/FoxA1 transcriptional repression rather than mutation, that were predictive of recurrence (Figures 4B and 5A–C) (48). As exact mechanisms of CREB1-mediated transcriptional repression remain elusive, the therapeutic implications of this prognostic gene panel are undetermined (14). Interestingly, the lowest collective expression of Panel B genes generally occurred in patients with the strongest collective expression of Panel A genes (Figure 5A and B). This seems to indicate that heightened CREB1/FoxA1 activity results in coordinated up- and downregulation events and that focusing on just a few genes that universally indicate CREB1/FoxA1 signaling could be sufficient for characterizing a given patient's risk. Based on its strong performance in prediction models, we suggest that Panel B gene expression could also be further developed into a tool to define an aggressive subset of primary prostate cancers in patients destined to relapse and who may benefit from trials of adjuvant therapy.

Tremendous enthusiasm has developed for the use of circulating tumor cells for real-time monitoring of dynamic events in both primary and metastatic cancer settings without the need for invasive tissue biopsy. A great deal has been learned through the analysis of circulating tumor content regarding the prevalence and clonality of common prostate cancer deletions and mutations in cases with multiple metastatic foci (62), the enhanced expression of EMT-related genes in CRPC patients (21), AR mutation and amplification status (63,64) and sustained AR signaling in the presence of hormone therapy (65). Our analysis showed that Panel A and B expression values were similar across recurrent prostate cancer patients regardless of whether or not they have developed resistance to antiandrogen therapy (Supplementary Figure S7A–C), thus they may have limited value beyond their strong performance in the primary cancer setting for predicting recurrence. Some controversy exists relating to the number of CTCs that can be isolated from primary versus metastatic prostate cancer pa-

tients (66), but future efforts should be made to determine whether CTC gene expression analysis could be applied to primary prostate cancer patients for the prediction of subsequent recurrence.

Finally, our findings collectively suggest that pCREB1 alone may not be an all-inclusive indicator of aggressive prostate cancer. While the phosphorylation of CREB1 is a partial marker of CREB1 transcriptional activity with demonstrated utility in identifying aggressive disease (50,67), it does not account for the phosphorylation-independent mechanisms of transactivation, which we now see can be potentiated by the cooperative function of FoxA1 and by the co-regulatory role of MED1. Thus, measuring total CREB1 transcriptional output, or that of a representative subset of disease-relevant genes, will likely afford increased sensitivity in predicting outcomes over pCREB1 levels alone.

SUPPLEMENTARY DATA

Supplementary Data are available at NAR Online.

ACKNOWLEDGEMENTS

Authors' contributions: B.S. and Q.W. designed this study. B.S., D.W. and Z.C. performed ChIP-seq and RNA-seq experiments. B.S., X.L., Z.Y. and V.X.J. analyzed ChIP-seq and RNA-seq data. B.S., Z.C., H.L.-N., P.J.G. and S.K.C. designed and conducted analyses of predictive gene panels. C.-L.C. and T.H.-M.H. designed the CTC analysis. D.M. recruited patients for the CTC study. C.-M.W., A.M.H., J.L. and C.-L.C. prepared samples and performed CTC gene expression analysis. B.S. and C.-L.L. performed data analysis of CTC results. B.S. performed inhibitor studies. B.S. and Q.W. wrote the manuscript with input from D.W., C.-L.C., P.J.G., S.K.C., V.X.J. and T.H.-M.H.

FUNDING

Department of Defense [W81XWH-12-1-0615 to Q.W.]; National Institutes of Health/National Cancer Institute [R01CA151979 to Q.W., U54CA113001 to T.H-M.H., 1F31CA180535-01A1 to B.S.]; 2011 V Foundation V Scholar Award (to Q.W.); The Ohio State University Comprehensive Cancer Center (OSUCCC) Pelotonia Idea Award (to Q.W.); OSUCCC Pelotonia Graduate Fellowship Program (to B.S.). Funding for open access charge: National Institutes of Health/National Cancer Institute [R01CA151979 to Q.W.].
Conflict of interest statement. None declared.

REFERENCES

1. Grasso,C.S., Wu,Y.M., Robinson,D.R., Cao,X., Dhanasekaran,S.M., Khan,A.P., Quist,M.J., Jing,X., Lonigro,R.J., Brenner,J.C. *et al.* (2012) The mutational landscape of lethal castration-resistant prostate cancer. *Nature*, **487**, 239–243.
2. Barbieri,C.E., Baca,S.C., Lawrence,M.S., Demichelis,F., Blattner,M., Theurillat,J.P., White,T.A., Stojanov,P., Van Allen,E., Stransky,N. *et al.* (2012) Exome sequencing identifies recurrent SPOP, FOXA1 and MED12 mutations in prostate cancer. *Nat. Genet.*, **44**, 685–689.
3. Baca,S.C., Prandi,D., Lawrence,M.S., Mosquera,J.M., Romanel,A., Drier,Y., Park,K., Kitabayashi,N., MacDonald,T.Y., Ghandi,M. *et al.* (2013) Punctuated evolution of prostate cancer genomes. *Cell*, **153**, 666–677.
4. Arora,V.K., Schenkein,E., Murali,R., Subudhi,S.K., Wongvipat,J., Balbas,M.D., Shah,N., Cai,L., Efstathiou,E., Logothetis,C. *et al.* (2013) Glucocorticoid receptor confers resistance to antiandrogens by bypassing androgen receptor blockade. *Cell*, **155**, 1309–1322.
5. Pflueger,D., Terry,S., Sboner,A., Habegger,L., Esgueva,R., Lin,P.C., Svensson,M.A., Kitabayashi,N., Moss,B.J., MacDonald,T.Y. *et al.* (2011) Discovery of non-ETS gene fusions in human prostate cancer using next-generation RNA sequencing. *Genome Res.*, **21**, 56–67.
6. Taylor,B.S., Schultz,N., Hieronymus,H., Gopalan,A., Xiao,Y., Carver,B.S., Arora,V.K., Kaushik,P., Cerami,E., Reva,B. *et al.* (2010) Integrative genomic profiling of human prostate cancer. *Cancer Cell*, **18**, 11–22.
7. Robinson,D., Van Allen,E.M., Wu,Y.M., Schultz,N., Lonigro,R.J., Mosquera,J.M., Montgomery,B., Taplin,M.E., Pritchard,C.C., Attard,G. *et al.* (2015) Integrative clinical genomics of advanced prostate cancer. *Cell*, **161**, 1215–1228.
8. Lalonde,E., Ishkanian,A.S., Sykes,J., Fraser,M., Ross-Adams,H., Erho,N., Dunning,M.J., Halim,S., Lamb,A.D., Moon,N.C. *et al.* (2014) Tumour genomic and microenvironmental heterogeneity for integrated prediction of 5-year biochemical recurrence of prostate cancer: a retrospective cohort study. *Lancet Oncol.*, **15**, 1521–1532.
9. Hieronymus,H., Schultz,N., Gopalan,A., Carver,B.S., Chang,M.T., Xiao,Y., Heguy,A., Huberman,K., Bernstein,M., Assel,M. *et al.* (2014) Copy number alteration burden predicts prostate cancer relapse. *Proc. Natl. Acad. Sci. U.S.A.*, **111**, 11139–11144.
10. Zhang,C., Wang,L., Wu,D., Chen,H., Chen,Z., Thomas-Ahner,J.M., Zynger,D.L., Eeckhoute,J., Yu,J., Luo,J. *et al.* (2011) Definition of a FoxA1 Cistrome that is crucial for G1 to S-phase cell-cycle transit in castration-resistant prostate cancer. *Cancer Res.*, **71**, 6738–6748.
11. Manna,P.R., Chandrala,S.P., Jo,Y. and Stocco,D.M. (2006) cAMP-independent signaling regulates steroidogenesis in mouse Leydig cells in the absence of StAR phosphorylation. *J. Mol. Endocrinol.*, **37**, 81–95.
12. Huang,W.C., Wu,D., Xie,Z., Zhau,H.E., Nomura,T., Zayzafoon,M., Pohl,J., Hsieh,C.L., Weitzmann,M.N., Farach-Carson,M.C. *et al.* (2006) beta2-microglobulin is a signaling and growth-promoting factor for human prostate cancer bone metastasis. *Cancer Res.*, **66**, 9108–9116.
13. Altarejos,J.Y. and Montminy,M. (2011) CREB and the CRTC co-activators: sensors for hormonal and metabolic signals. *Nat. Rev. Mol. Cell Biol.*, **12**, 141–151.
14. Johannessen,M., Delghandi,M.P. and Moens,U. (2004) What turns CREB on? *Cell. Signal.*, **16**, 1211–1227.
15. Chen,Z., Zhang,C., Wu,D., Chen,H., Rorick,A., Zhang,X. and Wang,Q. (2011) Phospho-MED1-enhanced UBE2C locus looping drives castration-resistant prostate cancer growth. *EMBO J.*, **30**, 2405–2419.
16. Wang,Q., Li,W., Zhang,Y., Yuan,X., Xu,K., Yu,J., Chen,Z., Beroukhim,R., Wang,H., Lupien,M. *et al.* (2009) Androgen receptor regulates a distinct transcription program in androgen-independent prostate cancer. *Cell*, **138**, 245–256.
17. Xu,K., Wu,Z.J., Groner,A.C., He,H.H., Cai,C., Lis,R.T., Wu,X., Stack,E.C., Loda,M., Liu,T. *et al.* (2012) EZH2 oncogenic activity in castration-resistant prostate cancer cells is Polycomb-independent. *Science*, **338**, 1465–1469.
18. Culig,Z., Hoffmann,J., Erdel,M., Eder,I.E., Hobisch,A., Hittmair,A., Bartsch,G., Utermann,G., Schneider,M.R., Parczyk,K. *et al.* (1999) Switch from antagonist to agonist of the androgen receptor bicalutamide is associated with prostate tumour progression in a new model system. *Br. J. Cancer*, **81**, 242–251.
19. Wu,D., Sunkel,B., Chen,Z., Liu,X., Ye,Z., Li,Q., Grenade,C., Ke,J., Zhang,C., Chen,H. *et al.* (2014) Three-tiered role of the pioneer factor GATA2 in promoting androgen-dependent gene expression in prostate cancer. *Nucleic Acids Res.*, **42**, 3607–3622.
20. Osmulski,P., Mahalingam,D., Gaczynska,M.E., Liu,J., Huang,S., Horning,A.M., Wang,C.-M., Thompson,I.M., Huang,T.H.-M. and Chen,C.-L. (2014) Nanomechanical biomarkers of single circulating tumor cells for detection of castration resistant prostate cancer. *Prostate*, **74**, 1297–1307.

21. Chen,C.L., Mahalingam,D., Osmulski,P., Jadhav,R.R., Wang,C.M., Leach,R.J., Chang,T.C., Weitman,S.D., Kumar,A.P., Sun,L. *et al.* (2013) Single-cell analysis of circulating tumor cells identifies cumulative expression patterns of EMT-related genes in metastatic prostate cancer. *Prostate*, **73**, 813–826.
22. Glinsky,G.V., Glinskii,A.B., Stephenson,A.J., Hoffman,R.M. and Gerald,W.L. (2004) Gene expression profiling predicts clinical outcome of prostate cancer. *J. Clin. Invest.*, **113**, 913–923.
23. Cerami,E., Gao,J., Dogrusoz,U., Gross,B.E., Sumer,S.O., Aksoy,B.A., Jacobsen,A., Byrne,C.J., Heuer,M.L., Larsson,E. *et al.* (2012) The cBio cancer genomics portal: an open platform for exploring multidimensional cancer genomics data. *Cancer Discov.*, **2**, 401–404.
24. Martianov,I., Choukrallah,M.A., Krebs,A., Ye,T., Legras,S., Rijkers,E., Ijcken,W., Jost,B., Sassone-Corsi,P. and Davidson,I. (2010) Cell-specific occupancy of an extended repertoire of CREM and CREB binding loci in male germ cells. *BMC Genomics*, **11**, 530–545.
25. He,H.H., Meyer,C.A., Shin,H., Bailey,S.T., Wei,G., Wang,Q., Zhang,Y., Xu,K., Ni,M., Lupien,M. *et al.* (2010) Nucleosome dynamics define transcriptional enhancers. *Nat. Genet.*, **42**, 343–347.
26. Calo,E. and Wysocka,J. (2013) Modification of enhancer chromatin: what, how, and why? *Mol. Cell*, **49**, 825–837.
27. McLean,C.Y., Bristor,D., Hiller,M., Clarke,S.L., Schaar,B.T., Lowe,C.B., Wenger,A.M. and Bejerano,G. (2010) GREAT improves functional interpretation of cis-regulatory regions. *Nat. Biotechnol.*, **28**, 495–501.
28. Liang,J., Lacroix,L., Gamot,A., Cuddapah,S., Queille,S., Lhoumaud,P., Lepetit,P., Martin,P.G., Vogelmann,J., Court,F. *et al.* (2014) Chromatin immunoprecipitation indirect peaks highlight long-range interactions of insulator proteins and Pol II pausing. *Mol. Cell*, **53**, 672–681.
29. Everett,L.J., Le Lay,J., Lukovac,S., Bernstein,D., Steger,D.J., Lazar,M.A. and Kaestner,K.H. (2013) Integrative genomic analysis of CREB defines a critical role for transcription factor networks in mediating the fed/fasted switch in liver. *BMC Genomics*, **14**, 337–352.
30. Gerstein,M.B., Kundaje,A., Hariharan,M., Landt,S.G., Yan,K.K., Cheng,C., Mu,X.J., Khurana,E., Rozowsky,J., Alexander,R. *et al.* (2012) Architecture of the human regulatory network derived from ENCODE data. *Nature*, **489**, 91–100.
31. Lupien,M., Eeckhoute,J., Meyer,C.A., Wang,Q., Zhang,Y., Li,W., Carroll,J.S., Liu,X.S. and Brown,M. (2008) FoxA1 translates epigenetic signatures into enhancer-driven lineage-specific transcription. *Cell*, **132**, 958–970.
32. Theodorou,V., Stark,R., Menon,S. and Carroll,J.S. (2013) GATA3 acts upstream of FOXA1 in mediating ESR1 binding by shaping enhancer accessibility. *Genome Res.*, **23**, 12–22.
33. Sahu,B., Laakso,M., Ovaska,K., Mirtti,T., Lundin,J., Rannikko,A., Sankila,A., Turunen,J.P., Lundin,M., Konsti,J. *et al.* (2011) Dual role of FoxA1 in androgen receptor binding to chromatin, androgen signalling and prostate cancer. *EMBO J.*, **30**, 3962–3976.
34. Rhodes,D.R., Yu,J., Shanker,K., Deshpande,N., Varambally,R., Ghosh,D., Barrette,T., Pandey,A. and Chinnaiyan,A.M. (2004) ONCOMINE: a cancer microarray database and integrated data-mining platform. *Neoplasia*, **6**, 1–6.
35. Cancer Genome Atlas Network . (2012) Comprehensive molecular characterization of human colon and rectal cancer. *Nature*, **487**, 330–337.
36. Cancer Genome Atlas Network. (2012) Comprehensive molecular portraits of human breast tumours. *Nature*, **490**, 61–70.
37. Cuzick,J., Swanson,G.P., Fisher,G., Brothman,A.R., Berney,D.M., Reid,J.E., Mesher,D., Speights,V.O., Stankiewicz,E., Foster,C.S. *et al.* (2011) Prognostic value of an RNA expression signature derived from cell cycle proliferation genes in patients with prostate cancer: a retrospective study. *Lancet Oncol.*, **12**, 245–255.
38. Aytes,A., Mitrofanova,A., Lefebvre,C., Alvarez,M.J., Castillo-Martin,M., Zheng,T., Eastham,J.A., Gopalan,A., Pienta,K.J., Shen,M.M. *et al.* (2014) Cross-species regulatory network analysis identifies a synergistic interaction between FOXM1 and CENPF that drives prostate cancer malignancy. *Cancer Cell*, **25**, 638–651.
39. Lapointe,J., Li,C., Higgins,J.P., van de Rijn,M., Bair,E., Montgomery,K., Ferrari,M., Egevad,L., Rayford,W., Bergerheim,U. *et al.* (2004) Gene expression profiling identifies clinically relevant subtypes of prostate cancer. *Proc. Natl. Acad. Sci. U.S.A.*, **101**, 811–816.
40. Knezevic,D., Goddard,A.D., Natraj,N., Cherbavaz,D.B., Clark-Langone,K.M., Snable,J., Watson,D., Falzarano,S.M., Magi-Galluzzi,C., Klein,E.A. *et al.* (2013) Analytical validation of the Oncotype DX prostate cancer assay - a clinical RT-PCR assay optimized for prostate needle biopsies. *BMC Genomics*, **14**, 690–701.
41. Aung,C.S., Hill,M.M., Bastiani,M., Parton,R.G. and Parat,M.O. (2011) PTRF-cavin-1 expression decreases the migration of PC3 prostate cancer cells: role of matrix metalloprotease 9. *Eur. J. Cell Biol.*, **90**, 136–142.
42. Nassar,Z.D., Moon,H., Duong,T., Neo,L., Hill,M.M., Francois,M., Parton,R.G. and Parat,M.O. (2013) PTRF/Cavin-1 decreases prostate cancer angiogenesis and lymphangiogenesis. *Oncotarget*, **4**, 1844–1855.
43. Gober,M.D., Smith,C.C., Ueda,K., Toretsky,J.A. and Aurelian,L. (2003) Forced expression of the H11 heat shock protein can be regulated by DNA methylation and trigger apoptosis in human cells. *J. Biol. Chem.*, **278**, 37600–37609.
44. Yang,C., Hayashida,T., Forster,N., Li,C., Shen,D., Maheswaran,S., Chen,L., Anderson,K.S., Ellisen,L.W., Sgroi,D. *et al.* (2011) The integrin alpha(v)beta(3–5) ligand MFG-E8 is a p63/p73 target gene in triple-negative breast cancers but exhibits suppressive functions in ER(+) and erbB2(+) breast cancers. *Cancer Res.*, **71**, 937–945.
45. Thomassen,M., Tan,Q. and Kruse,T.A. (2009) Gene expression meta-analysis identifies chromosomal regions and candidate genes involved in breast cancer metastasis. *Breast Cancer Res. Treat.*, **113**, 239–249.
46. Vainio,P., Gupta,S., Ketola,K., Mirtti,T., Mpindi,J.P., Kohonen,P., Fey,V., Perala,M., Smit,F., Verhaegh,G. *et al.* (2011) Arachidonic acid pathway members PLA2G7, HPGD, EPHX2, and CYP4F8 identified as putative novel therapeutic targets in prostate cancer. *Am. J. Pathol.*, **178**, 525–536.
47. Gibbs,G.M., Roelants,K. and O'Bryan,M.K. (2008) The CAP superfamily: cysteine-rich secretory proteins, antigen 5, and pathogenesis-related 1 proteins–roles in reproduction, cancer, and immune defense. *Endocr. Rev.*, **29**, 865–897.
48. Davoli,T., Xu,A.W., Mengwasser,K.E., Sack,L.M., Yoon,J.C., Park,P.J. and Elledge,S.J. (2013) Cumulative haploinsufficiency and triplosensitivity drive aneuploidy patterns and shape the cancer genome. *Cell*, **155**, 948–962.
49. Vogelstein,B., Papadopoulos,N., Velculescu,V.E., Zhou,S., Diaz,L.A. Jr and Kinzler,K.W. (2013) Cancer genome landscapes. *Science*, **339**, 1546–1558.
50. Kumar,A.P., Bhaskaran,S., Ganapathy,M., Crosby,K., Davis,M.D., Kochunov,P., Schoolfield,J., Yeh,I.T., Troyer,D.A. and Ghosh,R. (2007) Akt/cAMP-responsive element binding protein/cyclin D1 network: a novel target for prostate cancer inhibition in transgenic adenocarcinoma of mouse prostate model mediated by Nexrutine, a Phellodendron amurense bark extract. *Clin. Cancer Res.*, **13**, 2784–2794.
51. Swarthout,J.T., Tyson,D.R., Jefcoat,S.C. Jr and Partridge,N.C. (2002) Induction of transcriptional activity of the cyclic adenosine monophosphate response element binding protein by parathyroid hormone and epidermal growth factor in osteoblastic cells. *J. Bone Miner. Res.*, **17**, 1401–1407.
52. Parker,D., Ferreri,K., Nakajima,T., LaMorte,V.J., Evans,R., Koerber,S.C., Hoeger,C. and Montminy,M.R. (1996) Phosphorylation of CREB at Ser-133 induces complex formation with CREB-binding protein via a direct mechanism. *Mol. Cell. Biol.*, **16**, 694–703.
53. Allen,B.L. and Taatjes,D.J. (2015) The Mediator complex: a central integrator of transcription. *Nat. Rev. Mol. Cell Biol.*, **16**, 155–166.
54. Pandey,P.K., Udayakumar,T.S., Lin,X., Sharma,D., Shapiro,P.S. and Fondell,J.D. (2005) Activation of TRAP/mediator subunit TRAP220/Med1 is regulated by mitogen-activated protein kinase-dependent phosphorylation. *Mol. Cell. Biol.*, **25**, 10695–10710.
55. Hu,R., Lu,C., Mostaghel,E.A., Yegnasubramanian,S., Gurel,M., Tannahill,C., Edwards,J., Isaacs,W.B., Nelson,P.S., Bluemn,E. *et al.* (2012) Distinct transcriptional programs mediated by the ligand-dependent full-length androgen receptor and its splice variants in castration-resistant prostate cancer. *Cancer Res.*, **72**, 3457–3462.
56. Cao,B., Qi,Y., Zhang,G., Xu,D., Zhan,Y., Alvarez,X., Guo,Z., Fu,X., Plymate,S.R., Sartor,O. *et al.* (2014) Androgen receptor splice

variants activating the full-length receptor in mediating resistance to androgen-directed therapy. *Oncotarget*, **5**, 1646–1656.
57. Chhabra,A., Fernando,H., Watkins,G., Mansel,R.E. and Jiang,W.G. (2007) Expression of transcription factor CREB1 in human breast cancer and its correlation with prognosis. *Oncol. Rep.*, **18**, 953–958.
58. Seo,H.S., Liu,D.D., Bekele,B.N., Kim,M.K., Pisters,K., Lippman,S.M., Wistuba,II and Koo,J.S. (2008) Cyclic AMP response element-binding protein overexpression: a feature associated with negative prognosis in never smokers with non-small cell lung cancer. *Cancer Res.*, **68**, 6065–6073.
59. Wu,D., Zhau,H.E., Huang,W.C., Iqbal,S., Habib,F.K., Sartor,O., Cvitanovic,L., Marshall,F.F., Xu,Z. and Chung,L.W. (2007) cAMP-responsive element-binding protein regulates vascular endothelial growth factor expression: implication in human prostate cancer bone metastasis. *Oncogene*, **26**, 5070–5077.
60. Xiao,X., Li,B.X., Mitton,B., Ikeda,A. and Sakamoto,K.M. (2010) Targeting CREB for cancer therapy: friend or foe. *Curr. Cancer Drug Targets*, **10**, 384–391.
61. Wu,C.L., Schroeder,B.E., Ma,X.J., Cutie,C.J., Wu,S., Salunga,R., Zhang,Y., Kattan,M.W., Schnabel,C.A., Erlander,M.G. *et al.* (2013) Development and validation of a 32-gene prognostic index for prostate cancer progression. *Proc. Natl. Acad. Sci. U.S.A.*, **110**, 6121–6126.
62. Carreira,S., Romanel,A., Goodall,J., Grist,E., Ferraldeschi,R., Miranda,S., Prandi,D., Lorente,D., Frenel,J.S., Pezaro,C. *et al.* (2014) Tumor clone dynamics in lethal prostate cancer. *Sci. Transl. Med.*, **6**, 254ra125.
63. Leversha,M.A., Han,J., Asgari,Z., Danila,D.C., Lin,O., Gonzalez-Espinoza,R., Anand,A., Lilja,H., Heller,G., Fleisher,M. *et al.* (2009) Fluorescence in situ hybridization analysis of circulating tumor cells in metastatic prostate cancer. *Clin. Cancer Res.*, **15**, 2091–2097.
64. Shaffer,D.R., Leversha,M.A., Danila,D.C., Lin,O., Gonzalez-Espinoza,R., Gu,B., Anand,A., Smith,K., Maslak,P., Doyle,G.V. *et al.* (2007) Circulating tumor cell analysis in patients with progressive castration-resistant prostate cancer. *Clin. Cancer Res.*, **13**, 2023–2029.
65. Miyamoto,D.T., Lee,R.J., Stott,S.L., Ting,D.T., Wittner,B.S., Ulman,M., Smas,M.E., Lord,J.B., Brannigan,B.W., Trautwein,J. *et al.* (2012) Androgen receptor signaling in circulating tumor cells as a marker of hormonally responsive prostate cancer. *Cancer Discov.*, **2**, 995–1003.
66. Alix-Panabieres,C. and Pantel,K. (2014) Challenges in circulating tumour cell research. *Nat. Rev. Cancer*, **14**, 623–631.
67. Hassan,S., Karpova,Y., Flores,A., D'Agostino,R. Jr, Danhauer,S.C., Hemal,A. and Kulik,G. (2014) A pilot study of blood epinephrine levels and CREB phosphorylation in men undergoing prostate biopsies. *Int. Urol. Nephrol.*, **46**, 505–510.